https://doi.org/10.1016/j.istruc.2021.05.052

A Comprehensive Numerical Approach for Modelling Blind-Bolted CFST Connections

Partha Pratim DEBNATH and Tak-Ming CHAN*

Department of Civil and Environmental Engineering,

The Hong Kong Polytechnic University, Kowloon, Hong Kong

**tak-ming.chan@polyu.edu.hk*

Abstract

Conducting numerical investigation for the behaviour of a blind-bolted connection with concrete-filled steel tube (CFST) and an open steel section could emerge with several convergence issues due to its complex mechanism and interactions between the connection components. This paper attempts to identify and address these issues and provide reliable solution techniques that can be adopted to achieve convergence and accurately predict the behaviour of blind-bolted CFST connections. Three different types of blind-bolts, which are currently used in experimental research, have been considered in this study. Primarily, the paper addresses the blind-bolt modelling aspects, application of bolt preload, identification of interaction surfaces, use of mass-scaling option, system energy issues and non-linear material modelling. For accurate representation of concrete compressive crushing and tensile cracking, the existing available material models with damage criteria have also been discussed. Sensitivity analyses have also been conducted for such connections which will complement the reliability of the numerical models. The generated numerical models are in good agreement with existing experimental counterparts. Thus, the techniques discussed can be adopted for a comprehensive modelling and understanding of blind-bolted CFST connections with reduced computational cost, and help making rational design for future experimental tests.

Keywords

Blind-bolts, CFST columns, numerical analysis, bolted connections, anchored bolts

1. Introduction

The use of concrete-filled steel tube (CFST) columns in high-rise structures have undergone a rapid rise due to several advantages, like higher strength, enhanced ductility, improved fire resistance, aesthetics etc. as compared to simple steel or concrete structures. In CFST, the strength of the concrete core is enhanced due to the confinement provided by the steel tube, and infill concrete can help delay the buckling of the external tube [1-3]. The behaviour of CFST having different cross-section shapes with high-strength materials have also been studied and the performance is well pronounced [4, 5]. The CFST columns are usually connected to the open section steel beams via welds or bolts, or a combination of both. In welded connections, the steel beam is welded to the column face and in bolted connection, bolts or shear studs are used to penetrate the column tube. In recent years, the use of bolts over welds is being preferred due to many advantages like easier fabrication and lower cost, as it involves semi-skilled labour unlike welding. Bolting can also eliminate the heat effect, that arises due to welding which induces stress concentration in the welded zone [6]. The use of bolts is increasingly becoming popular for rapid in-situ constructions like modular integrated construction (MiC) or modular steel construction (MSC), and modifications in bolts are being explored to accommodate desired applications [7, 8]. Bolts are generally assembled in different configurations with end-plates that connect the steel tube with the CFST column. However, the use of standard bolts is not easy to connect hollow steel tubes due to limited access from inside the tube which is required for tightening the bolts. To overcome this issue, the so-called blind-bolt was proposed. Numerous experimental investigations can be found in the literature involving blind-bolted connections with various types of end plates like the flush end-plate, extended end-plate, T-stub connection and L-stub connections [9-13]. These investigations reported that the connection performance is influenced by thickness of end-plate, column geometry, steel tube strength, bolt diameter, bolt pretension force, static and cyclic loading.

Conducting such experimental investigations is deemed necessary to understand the failure mechanism and behaviour of bolted CFST connections. In addition to experimental investigations, adopting numerical tools can be a good alternative that helps saving cost and time intensive laboratory experiments. The use of finite element analyses (FEA) is a common approach adopted to predict the behaviour of any structural system, and have gained much popularity due to better graphical user interface, high computational capacity processors, diverse range of material models, excellent visualization of local and global deformation that commercial FEA software like ABAQUS [14] offers. Numerical analyses can also overcome certain limitations in the experimental setup and can complement existing experimental databases with extensive parametric studies. The combined use of FEA, along with experimental testing can produce more meaningful results and enable future laboratory testing to be designed more coherently. However, the reliability of the numerical model depends on the accuracy of the developed model and correct defining of all boundary conditions. The situation becomes challenging for complex systems like blind-bolted CFST connections. Though, numerical studies have been conducted involving bolts and CFST connections on structural performance point-of-view [15-19], but a comprehensive discussion on modelling aspects of blind-bolted CFST connection is still rare.

This paper addresses the challenges in numerical FE modelling of blind-bolted CFST connections, which have complex geometry with surface interaction issues, non-linear material modelling of steel and concrete for generating accurate FE models. Issues involving meshing, achieving bolt pretension, mass-scaling, applying correct loading rate, pseudo-static analysis, concrete tensile damage, tackling non-convergence are discussed elaborately in this paper. It is to be noted that proper modelling of compressive crushing and tensile crack of concrete core confined by the steel tube is necessary to accurately capture the concrete failure modes under different loading condition. The paper also presents how existing models of concrete tensile

damage and fracture energy definition can influence the numerical behaviour. Further, the study also explains step-by-step method to achieve converge using a dynamic method for quasi-static solution. To provide a wider acceptability of the study, three different types of blind-bolts, called the headed anchored blind-bolt (HABB), extended hollo-bolt (EHB) and the Slip-critical blind-bolt (SCBB), currently used in experimental research have been considered with hollow and CFST columns. The developed FE models have been validated against the experimental results to assess the reliability of the models. The techniques discussed in the paper can be adopted not only for modelling of single blind-bolted CFST (or hollow tube) connections, but also for group blind-bolted CFST (or hollow tube) connections. At the end, major observations are reported that can be used for developing blind-bolted hollow or CFST connections with sufficient accuracy to understand the connection behaviour and help in making rational design for future experimental tests.

2. Summary of bolted-connection tensile tests

In general practice, studs or cogged bars fixed inside hollow steel tube columns are used to connect with open section beams, however, it was realised that the installation of such a connection is cumbersome. The blind-bolts can overcome this limitation, since they are easily handled, can be inserted from one side of the column face, and can be tightened with the desired bolt torque without accessing the inside of the steel tube.

To study the performance and behaviour of such blind-bolted connections with hollow and CFST columns, researchers especially in regions like Australia, China, Malaysia and the United Kingdom have conducted various experimental studies that involve the use of different types of blind-bolts. In addition to studying the behaviour of various types of stub and end-plate bolted connections with CFST columns, researchers have also investigated the performance of the connections with special attention to the blind-bolts and have proposed several

modifications to enhance their performance. The blind bolts manufactured by AJAX Fasteners (Australia) [20] were modified by replacing the standard bolt shank with an elongated shank, fitted with a circular nut at the shank tip. This modified blind-bolt were called as headed anchored blind-bolts (HABB). The HABBs were investigated under tensile pull-out tests by Oktavianus *et al.* and Agheshlui *et al.* [21, 22] and observed to have higher strength and stiffness as compared to the standard AJAX blind bolts.

Secondly, the hollo-bolt which is another type of blind-bolt, manufactured by Lindapter International (UK) [23] was modified by extending the shank length and attaching a headed nut and named as extended hollo-bolts (EHB) by Pitrakkos *et al.* [24]. The tensile performance of EHB was investigated by Pitrakkos *et al.*, Tizani *et al.*, and Debnath *et al.* [24-27] and observed to have enhanced composite behaviour with significant concrete contribution under tensile pull-out loading. Connections with another novel blind-bolt called the slip-critical blind-bolt (SCBB) proposed by Wang *et al.* [28] was also investigated and have reported to possess good hysteretic properties and behave as moment-resisting connections [29, 30].

In the present research study, the previously mentioned three types of blind-bolts, i.e., HABB, EHB and the SCBB have been considered, which are shown in Fig. 1. These bolts have been used in conjunction either with hollow or CFST columns in the experimental works of Agheshlui *et al.* [22] using HABB, Pitrakkos *et al.* [24] using EHB, and Xu *et al.* [30] using SCBB, that have been adopted to serve as reference for developing and validating numerical techniques. It is worth mentioning that the three experimental testing programs adopted for the study had monotonic tensile pull-out loading applied to a single or group blind-bolted connection with various boundary conditions. The pull-out displacement was measured at the bolt head outside the tube. The experiments conducted using HABB [22] was with square CFST columns having connections with bolts of strength grade of 8.8 and diameter ranging from M16 to M24. The experimental specimens having connections with HABB bolts were

indexed as (test series)-(number of bolts and bolt diameter)-(location of bolt), for example, A-1M20-Mid. The test using EHB [24] bolts with concrete filled column sections consisted of connections having bolt of diameter M16 and M20 with strength grades of 8.8 and 10.9. The indexing for the test series with EHB bolts was presented as (type of bolt and diameter)-(total length of internal bolt)-(bolt grade and bolt batch)-(grade of concrete infill)-(specimen number), for example, EHB20-150-8.8F-C40-2. For the experiment conducted using SCBB [30] was with octagonal hollow steel tube having connections with M20 group bolts having strength grade of 10.9. The labelling for the specimens having connections using SCBB bolts was made as (specimen geometry)-(specimen width)-(column tube thickness)-(number of T-stubs), for example, Oct-W150-T4-S, where S represent a single T-stub. Accurate numerical models have been generated for these bolted connections and their modelling strategies have been elaborately discussed here. The experimental setup and the corresponding developed simplified numerical model, simulating the connection pull-out tests are presented in Fig. 2 and Fig. 3, respectively.

3. Comprehensive numerical modelling

This section discusses the FE analysis or numerical techniques adopted using the finite element software package ABAQUS [14]. All the components present in a blind-bolted hollow or CFST column connection are modelled with sufficient accuracy along with material damage modelling.

3.1. Blind-bolt connection modelling

In this research program, the blind-bolts have been modelled using the 3-dimensional 8-noded C3D8R solid element, which is a general-purpose linear brick element with reduced integration. In this method, the bolt head, nut, and shank can be modelled as a single unit to ease with the interactions between them and assuming no slip of nut from the bolt shank. The

148 other bolt components like the bolt sleeve and bolt washer were also modelled and contact
149 interactions between them were applied. The HABB type of bolt was modelled as two
150 components; where the bolt nut, head, shank, and washers form a single component, and the
151 sleeve forms another component. For EHB type of bolt, it was also simplified and modelled in
152 two units; the bolt head, bolt washer, bolt shank, fastener cone and the nut at the end are
153 modelled as a single unit and the expandable sleeve as another unit. In existing literature, the
154 hollo-bolts (and EHB) were modelled without the expandable sleeve which forms an important
155 component of the bolted connection. Under tensile loading, the expandable sleeve, which is
156 supported on the conical nut, transfers the load to the column tube wall by bearing. Also, since
157 the material grade of the sleeve component is different from the bolt shank, it is necessary to
158 model the sleeve as a separate part instance. From an experimental evidence [24], it is observed
159 that connection failure in hollow tubes occurred due to sleeve failure, and ignoring the sleeve
160 may not simulate the realistic behaviour. In addition to this, by omission of the expandable
161 sleeve in modelling, there will exist only concrete contribution arising due to the anchorage of
162 the EHB. The expandable sleeve, which gives rise to the steel tube-wall bearing, will not be
163 able to reflect in the FE behaviour of the connection strength and stiffness in case the
164 expandable sleeve is not modelled.

165 The SCBB bolt was modelled into four components; the bolt shank, bolt nut and head form a
166 single component, whereas the sleeve, washer and the split washer form the other three
167 components as shown in Fig. 4. The unmeshed FE models for the three types of bolt are
168 presented in Fig. 5. It is worth mentioning that the foldable steel washer in HABB and split-
169 washer in SCBB are the bearing components, however, the expandable sleeve forms the
170 bearing component in the hollo-bolt.

171

The simulation program for tensile test of bolted connection was initially attempted using Abaqus/Standard adopting both "static general" and "implicit" technique. However, a convergent solution could not be attained, and analysis ceased at significantly lower load, which is possibly caused by many interaction surfaces within the numerical model. Therefore, Abaqus/Explicit was adopted for all the simulations in the present study, which is further explained in later sections of the paper.

3.1.1. Bolt pretension load

As the bolted connections are required to be applied with bolt preload or bolt torque while installation, it is also required to replicate this load in the numerical models. As per Eurocode 3 [31], the design preload, $F_{p,Cd,}$ for M20 bolt of grade 8.8 and 10.9 is 124 kN and 155 kN respectively. The bolt design preload, $F_{p,Cd}$ is given as:

$$F_{p,Cd} = 0.7 f_{ub} A_s / \gamma_{M7} \quad (1)$$

Where, f_{ub} is the bolt ultimate tensile strength, A_s is the bolt tensile area and γ_{M7} is the partial safety factor.

To apply the bolt load or bolt pretension, the "bolt load" tool is not available in explicit dynamics solver, therefore the "initial temperature" load was used to induce the preload. In this technique of using temperature load, a thermal coefficient was applied to the bolt material and then a reference temperature was assigned to the bolt shank area. The application of reference temperature was made in the initial step and then a reduced temperature was applied in the next load step, which will lead to a contraction in the shank and thus induce the desired "preload". This was done by using the "Predefined Field Manager" option which was then "Propagated" to the next load steps. The location for applying the preload is shown in Fig. 5 for the three types of bolts being discussed here.

A comparison for the bolt pretension load using the “bolt load” and “temperature load” was made using standard and explicit analysis, respectively. This was done to confirm that the explicit solver using the “temperature load” was able to attain similar stress level as that of the corresponding “bolt load” in the implicit solver. For this comparison, a simple connection was modelled, with no additional bolt components except the bolt shank, bolt head and bolt nut, which were modelled as a single unit, and a steel tube with a hole, through which the bolt is attached. This simplest form of bolted connection was used for the comparison, as it is expected to achieve convergence due to the lesser number of interaction surfaces. The behaviour of this connection with “bolt load” and “temperature load” is presented in Fig.6, with the connection shown in the inset. As observed from Fig. 6, both techniques for applying preload produce force-displacement curves that are sufficiently similar in behaviour and thus, the temperature load in explicit solver can be used to induce the bolt preload.

To assess the stress achieved in the bolt shank after applying the bolt preload by using the temperature load, another comparison was carried out between the two models. For this assessment, a single step analysis was done, where bolt load Abaqus/standard and temperature load Abaqus/explicit was applied and checked for the stresses in the shank region. As observed from Fig. 7, the average stresses in both the bolt shanks show similar value of stress levels attained for a typical slip critical blind-bolt (SCBB). Inducing similar stress levels by use of temperature load indicates that it can be used for pre-tensioning of blind-bolts in the explicit solver.

A further comparison was made to understand the influence of bolts with and without the pretension load. For this study, an experimental specimen tested by Xu and Chan [30] was adopted to compare with numerical simulations with and without bolt pretension load a shown in Fig. 8. As observed, the model without bolt pretension can potentially underestimate the stiffness of the connection and the strength of the connection drops considerably, whereas the

model with equivalent bolt pretension has achieved similar deformation behaviour as that of the experimental result. Therefore, it would be necessary to model the blind-bolted connections with the required design preload for accurately predicting the behaviour as in the experimental tests.

3.1.2. Connection elements and meshing

The element types for concrete, steel endplate, bolt and its components have been modelled using the eight-node linear brick elements with reduced integration having hourglass control, referred to as C3D8R in ABAQUS. For modelling steel tubes, the shell element with six degrees of freedom at each node with reduced integration, referred to as S4R in ABAQUS was used as it is computationally more efficient due to a smaller number of degrees of freedom. As reported by Dai and Lam [32], for modelling steel tubes both solid and shell element can be used as the wall thickness is relatively small compared to other dimensions of the specimen, but for circular or elliptical tubes if shell element is used it would be difficult to follow the curved contact boundary and therefore C3D8 or C3D20 were used for any circular steel tubes.

The finite element meshing was based on sensitivity studies and the size of $d/2$ was found to be most effective for meshing concrete core and steel tube. For bolt components, the element mesh size of $d/4$ was observed to have the best results, where d is the bolt diameter. As the bolt is the smallest component in the connection system, the analysis results are governed by the bolt mesh size, and therefore the element mesh size for concrete core, steel tube and bolt components are defined in terms of bolt diameter. In complex composite bolted connection, the region comprising of bolts, open beam, endplate, steel tube and concrete, were modelled with the smallest element size i.e., the mesh size of the bolt component ($d/4$) to ensure better node-to-node interaction, more accurate capturing of deformation behaviour and avoid any

243 convergence issue, as shown in Fig.9. The region of finer mesh was assumed to be two times
244 the length of the connection, extended on both sides of the connection.

245 A study to analyse the influence of bolt mesh size was conducted, where three different mesh
246 sizes of (d/2.5), (d/2.85) and (d/4) were considered. The study was conducted using the tests
247 by Agheshlui *et al.* [22] and Pitrakkos *et al.* [24] where HABB and EHB bolts of size M20
248 were used. Thus, bolt mesh sizes of 5 mm, 7 mm and 8 mm were considered for this analysis.
249 As mentioned previously, the mesh sizes of steel tube and concrete core all were meshed with
250 the same size as that of the bolt mesh for a length of twice the connection length in both sides
251 of the connection, and this strategy was considered in this study as well. The behaviour of the
252 numerical model with varied bolt mesh size is shown in Fig. 10 (a) and Fig. 10 (b), which
253 shows that the post-yield behaviour is influenced by the bolt mesh size. The computer CPU
254 time required for analysis of the numerical models with different mesh sizes is presented in
255 Table 1 which shows that, the time required for the model having bolt mesh size of d/4 is almost
256 4-times more than the model having bolt mesh size of d/2.5.

257 The FE models with the mesh size of 5 mm or d/4 had the closest response with the
258 experimental counterpart but with a higher computational cost as compared to the simulations
259 using mesh sizes of (d/2.5) and (d/2.85). An attempt was made using a mesh size of d/5 or 4
260 mm, but using this size led to early cessation of the analysis as the ratio of deformation speed
261 to wave speed exceeds 1 in the elements, which generally occurs when the mesh size too small.
262 Also observed from the experimental tests, the failure mode for CFST using HABB was
263 governed by the concrete failure whereas, for the CFST with EHB connection was governed
264 by the bolt strength. Therefore, the force-displacement behaviour of the EHB connection
265 shown in Fig. 10 (b) there appears to be a slight deviation in the stiffness for the numerical
266 model having 5 mm mesh size as the behaviour was governed by the blind-bolt. In a realistic

situation, the global connection behaviour is not expected to be governed by the blind bolt, and therefore the mesh size will not significantly influence this stiffness.

The EHB bolt deformation behaviour using three mesh sizes are also shown in Fig. 11, where the bolt shank necking with a mesh size of 5 mm is predominant and replicates the experimental findings. The bolt with 8 mm mesh size is observed to have some stress concentration in the shank that is embedded in the concrete core and might have influenced the post-yield behaviour of the connection. From these observations, though with a comparatively higher computational cost, the bolt mesh size *d*/4 is found suitable for conducting the simulations as it best replicates the connection behaviour.

3.1.3. Connection interaction modelling

In addition to the above-mentioned aspects, the interaction properties and surface contact interactions for the components of the model need to be carefully defined and assigned. Generally, three different interaction properties (IP) were considered, here named as IP1, IP2 and IP3. The interaction property IP1 is defined as "hard" contact in a normal direction allowing separation after contact and a tangential behaviour with "penalty" friction behaviour with a friction coefficient. IP2 is a normal contact behaviour with a "hard" pressure-overclosure relationship allowing separation after contact and, IP3 is a tangential behaviour with "frictionless" friction formulation. The interaction properties were assigned using "surface-to-surface" contact available in ABAQUS/Explicit and switching between the "first surface" and "second surface" of the contact does not make any differences.

Varied by cases, there are numerous surface contact pairs in bolt tensile pull-out tests. The contact pairs for CFST having a connection with HABB can be listed as (a) steel tube – concrete infill, (b) bolt shank – steel tube, (c) bolt washer – steel tube, (d) bolt washer– concrete, and (e) bolt shank – concrete. For the CFST having connections using EHB, the contact pairs are

(a) steel tube – concrete infill, (b) stub plate – steel tube, (c) stub plate – bolt washer, (d) stub plate –sleeve, (e) bolt shank – concrete, (f) conical nut – concrete, (g) bolt head – concrete, (h) sleeve – concrete, (i) sleeve – bolt washer, and (j) conical nut – expanded part of the sleeve. The interaction surfaces for a hollow octagonal tube having connections using SCBB consists of (a) bolt nut – washer, (b) washer – endplate, (c) endplate – steel tube, (d) bolt sleeve – endplate, (e) bolt sleeve – steel tube, (f) bolt sleeve – split washer, (g) split washer – bolt head. If the steel tube having connection with SCBB also have infill concrete, then concrete surface interactions with the bolt components and tube wall will also arise, which are not considered in this study as the considered experiment was a hollow tube. The contact surfaces in bolted connections as discussed above are presented in Fig. 12.

For the connections with HABB and SCBB under tensile loading, the sleeve is observed to remain as a passive component, but the foldable washer (in HABB) and the split washer (in SCBB) are the key components that transfer the load to the steel tube wall by bearing. For the CFST column connection using HABB under tensile loading, it is observed that upon concrete cone failure due to the bolt anchorage, the load is gradually transferred to the column tube wall by bearing the foldable washer. Whereas when the CFST connection is composed of EHB, the expandable sleeve forms an active component under tensile loading. The expanded sleeve which is supported on the conical nut not only grips the tube wall with the stub plate, but also forms the load transferring component by bearing on the tube wall. Therefore, careful modelling of the foldable washer, expandable sleeve, and the split washer for HABB, EHB and SCBB respectively, is necessary for predicting the connection behaviour under tensile loading.

The influence of friction coefficient between the steel material and the concrete is an important factor for CFST columns specially when loaded via shear connections, where the load is transferred from the steel tube to the concrete core by contact bond strength. As observed in existing findings that the shear resistance of steel and concrete interface is not only dependent

316 on the geometry of the steel tube, but also steel-concrete interface condition [33, 34]. Therefore,
317 the influence of the frictional coefficient is studied for the bolted CFST connections under
318 tensile pull-out loading. The frictional coefficient between the two surfaces normally ranges
319 from 0.2 to 0.6 [12] and for the current program values of 0.4, 0.5 and 0.6 are adopted. The
320 load-displacement behaviour with these varied coefficients is presented in Fig. 13. As
321 observed, the frictional value had negligible influence until the load drops due to concrete
322 crushing. As the tube wall starts yielding under the pull-out load, the frictional coefficient
323 seems to have some influence, but this influence too can be disregarded as under the tensile
324 loading there exists no sliding between the solid elements against each other. But the relative
325 lateral motion of the two solid surfaces, like the steel tube and concrete surface is significantly
326 existent in a shear loading when the beam is usually welded to the CFST column outer surface,
327 and the influence of the frictional coefficient would be considerable. In addition to the steel-
328 to-concrete friction surfaces in the connection, the friction between the steel components, such
329 as column tube, end plate or stub plate, bolt, and its components were also considered and a
330 "penalty" friction coefficient of 0.4 was adopted.

331 **3.1.4. Boundary conditions**

332 It is observed in the literature that most of the experimental specimens for tensile pull-out tests
333 were larger than 1.0 meters in length. Such specimens with concrete infill, hollow steel tube
334 and with several pairs of blind-bolts with stub connection, the total number of elements, both
335 solid (C3D8R) and shell (S4R) can be exceedingly high. With such a huge number of elements,
336 the computational analysis can be very expensive and therefore taking the advantage of
337 geometric symmetry the specimens can be modelled as half or quarter model. To ascertain the
338 fact that a half or quarter model can represent an original size model, a comparison is made
339 with an experimental specimen. The model is shown in Fig.14 and their behaviour is presented
340 in Fig.15. For defining the half or quarter model, the symmetry boundary conditions need to

be applied along with end fixity conditions. The tensile loading applied can be replicated by applying a displacement control boundary condition in the bolt head or the stub component. From Fig. 14 and Fig. 15, it can be stated that the quarter scaled model not only sufficiently captures the behaviour of the full-scale model but also reduces the computational time by 5.7 times in case of the FE models for the test by Xu *at al.* [30]. In case a full model is adopted over a half or quarter model, assigning fixity conditions at the ends of the effective length of the CFST column would be necessary. In this study, the effective length is referred to the clear length of the column between the clamps made on the strong floor of the experimental setup. For the CFST columns the effect of tube imperfection was not considered, as due to the presence of infill concrete there is negligible influence of tube imperfection, which usually is an important factor for hollow steel tubes.

3.2. Steel material model

For the modelling of hollow steel tubes, bolts and their components in the current research program, the stress-strain material models proposed by Yun and Gardner [35] are used. In addition to the conventional elastic perfectly-plastic steel material model, there are several steel material models found in the literature [36, 37] that offer bilinear or multi-linear stress-strain curves. However, in the present study, the model proposed by Yun and Gardner [35] is adopted as extensive data from over 500 experimental stress-strain curves of hot-rolled steels have been analysed from all over the globe. Also, using a bilinear material model would be very inaccurate for steel materials having sharp yield point due to the existence of yield plateau, which cannot be captured in a bilinear model.

The bilinear plus nonlinear hardening model proposed by Yun and Gardner [35] developed predictive expressions for ultimate strain and strain hardening modulus that can represent the steel behaviour with significant accuracy. The bilinear plus nonlinear model that shows the yield plateau and strain hardening behaviour, which is used to model the steel components in

the current study, is shown in Fig.16. This model is observed to be suitable for advanced numerical simulations where capturing the gradual loss of stiffness is important. The full range of tensile strain for the bilinear and nonlinear hardening model is given as:

$$(\varepsilon) = \begin{cases} E_\varepsilon & for\ \varepsilon \le \varepsilon_y \\ f_y & for\ \varepsilon_y < \varepsilon \le \varepsilon_{sh} \\ f_y + (f_u - f_y)\left\{ K_1\left(\frac{\varepsilon-\varepsilon_{sh}}{\varepsilon_u-\varepsilon_{sh}}\right) + \frac{K_2\left(\frac{\varepsilon-\varepsilon_{sh}}{\varepsilon_u-\varepsilon_{sh}}\right)}{\left[1+K_3\left(\frac{\varepsilon-\varepsilon_{sh}}{\varepsilon_u-\varepsilon_{sh}}\right)^{K_4}\right]^{1/K_4}} \right\} & for\ \varepsilon_{sh} < \varepsilon \le \varepsilon_u \end{cases} \quad (2)$$

where, f_y is the steel yield stress, ε_y is the corresponding yield strain, ε_{sh} is the strain hardening strain, f_u is the ultimate yield stress, ε_u is the corresponding ultimate tensile strain, K_1, K_2, K_3 and K_4 are material coefficients which values are 0.4, 2, 400 and 5 respectively; and, ε_u and ε_{sh} are given by the following equations:

$$\varepsilon_u = 0.6\left(1 - \frac{f_y}{f_u}\right), \qquad \text{where, } \varepsilon_u \ge 0.06 \text{ for hot-rolled steels} \quad (3)$$

$$\varepsilon_{sh} = 0.1\frac{f_y}{f_u} - 0.055, \qquad \text{where, } 0.015 \le \varepsilon_u \le 0.03 \quad (4)$$

The above predictive equations are used to model the engineering stress and engineering strain, which later are converted to the true stress and true strain as per the following equations:

$$\sigma_T = \sigma(1 + \varepsilon) \quad (5)$$

$$\varepsilon_T = \ln(1 + \varepsilon) \quad (6)$$

where, σ_T and ε_T are true stress and true strain, respectively. A representative plot of engineering stress-strain and true stress-strain for steel grade of S355 is shown in Fig.17. In general, the tube for the CFST column, open section beam, stub components (end-plates) and high strength blind-bolts are the major steel components for this research and a representative true stress-strain behaviour based on the test specimen by [22] is presented in Fig 18. The

Young's modulus of elasticity E_s , for steel and bolt components is considered as 210 N/mm^2 and Poisson's ratio is considered as 0.3 as per [38] in absence of experimental data.

3.3. Concrete material model

3.3.1.Concrete plasticity model

This section discusses about the use of Concrete Damage Plasticity (CDP) model for representing the concrete non-linear behaviour in ABAQUS. Usually, the non-linear behaviour of concrete under a compression load can be modelled either by plasticity model, or damage model, or a combination of both [39]. The plasticity model is characterized by the formation of unrecoverable deformation after unloading on the specimen, whereas, the damage model is concerned with the reduction of elastic stiffness of concrete [40].The concrete damage plasticity (CDP) model which is commonly used for defining concrete is a continuum, smeared-crack model which combines both plasticity and damage and is mainly based on works by Lubliner *et al.* and Lee *et al*. [41, 42] . The CDP model provides a general capacity for modelling the behaviour of quasi-brittle materials in various forms of structures, where it adopts the concept of isotropic damaged elasticity in combination with isotropic tensile and compressive plasticity for the purpose of representing the inelastic behaviour of concrete. The CDP model also assumes concrete compressive crushing and concrete tensile cracking and the response of the model under uniaxial tensile loading is characterized by a linear-elastic stress-strain relationship until the value of the failure stress, and during this stress the micro-cracks starts forming in the concrete [40]. The subsequent progressive formation of macro cracks leading to further opening is captured with the help of a softening stress-strain relationship, this relationship is defined as the "tensile softening" by means of post-failure stress-strain relation or a fracture energy cracking criterion that can be applied in the software package.

The eccentricity $\in$ is adopted as a default value of 0.1. It is to be noted that with significant less value than 0.1 for $\in$ could lead to convergence issues [43]. For considering the evolution of concrete strength under both compression and tension, the concrete damage plasticity model uses the yield function of Lubliner *et al.* [41] along with the modifications proposed by Lee *et al.* [44]. $\left(\frac{\sigma_{b0}}{\sigma_{c0}}\right)$ is the ratio of initial equibiaxial compressive yield stress to initial uniaxial compressive yield stress, has the default value of 1.16 as per [43], which is reported to be the maximum value as observed by [41] with minimum being 1.10. K_c is defined as the ratio of von Mises equivalent stress on the tensile meridian to the compressive meridian which must satisfy the condition of $0.5 < K_c \leq 1.0$, where the default value is 2/3 in [43]. In a research conducted by Tao *et al.* [45], the two parameters, K_c and dilation angle, ψ is found to have a significant influence on the performance of concrete and have proposed the following two equations which have also been used in the current research:

$$K_c = \frac{5.5}{5+2(f_c')^{0.075}} \tag{7}$$

$$\psi = \begin{cases} 56.3(1-\xi) & \xi \leq 0.5 \\ 6.672e^{\frac{7.4}{4.64+\xi}} & \xi > 0.5 \end{cases} \tag{8}$$

where, ξ is the confinement factor given as:

$$\xi = \frac{A_s f_y}{A_c f_c'} \tag{9}$$

where, f_c' is the cylinder compressive strength of concrete, A_c is the cross-sectional area of concrete, f_y is the yield strength of the steel tube, and A_s is the cross-sectional area of the steel tube. As observed by Tao *et al.* [45], for rectangular columns, a value of 40° can be used for ψ as the axial load (N) versus axial strain (ε) curves of rectangular columns are not very sensitive to ψ when it is greater than 20°. A value of 40° is found to have the best predictions

for the ultimate strength of concrete for rectangular specimens. In this research program, Equation 8 was used only in case of any circular columns.

3.3.2. Concrete compressive behaviour

In recent years, based on numerical studies, various researchers [46-48] have proposed compressive stress-strain models to be used for modelling of confined concrete in finite element packages, and these models can be directly applied to obtain the strain hardening and softening function directly without the use of any subroutines. This approach can thus reduce the complexities in modelling confined concrete and can overcome converge issues in ABAQUS.

In the current research program, a new three-stage model to represent the concrete strain hardening and softening rule proposed by Tao *et al.* [45] is adopted. Fig.19 shows the proposed stress-strain model with the initial stage OA, the plateau AB, and the softening part BC. During the stage OA, there is negligible interaction between the concrete and steel tube, and thus the ascending curve from O to A is appropriate until the strength reaches the peak value of f_c'. The plateau AB represents the increased peak strain of concrete due to the confinement arising from the steel tube, and it is during this stage that any enhancement of concrete strength will be captured during simulation through the interaction between concrete and steel tube surface. Starting from point B, there is a softening region where enhanced ductility due to the presence of a steel tube is captured.

In the model proposed by[45], the portion OA is adopted from [49] and is given as follows:

$$\frac{\sigma}{f_c'} = \frac{A.X+B.X^2}{1+(A-2)X+(B+1)X^2} \qquad 0 < \varepsilon \leq \varepsilon_{c0} \tag{10}$$

where, $X = \frac{\varepsilon}{\varepsilon_{c0}}$; $A = \frac{E_c \varepsilon_{c0}}{f_c'}$; $B = \frac{(A-1)^2}{0.55} - 1$

The strain at peak stress under uniaxial compression ε_{c0} is computed as per the following equation proposed by Nicolo *et al.* [50] which is based on regression analysis of concrete uniaxial compression tests where f_c' ranged from 10 MPa to 100 MPa:

$$\varepsilon_{c0} = 0.00076 + \sqrt{(0.626 f_c' - 4.33) \times 10^{-7}} \tag{11}$$

where f_c' is expressed in N/mm^2.

The value of strain at point B in Fig. 19 is obtained by the following equation proposed by Samani *et al.* [49]:

$$\frac{\varepsilon_{cc}}{\varepsilon_{c0}} = e^k,\ k = (2.9224 - 0.00367 f_c')\left(\frac{f_B}{f_c'}\right)^{0.3124 + 0.02 f_c'} \tag{12}$$

where f_B is the confining stress provided to concrete at point B where ultimate strength of the concrete is reached.

The confining stress on the concrete starts developing after point B and as stated above, there is no confining pressure in the elastic range from O to A. The confining stress increases after the yielding of steel and once the ultimate strength is reached the confining stress is stable or increases depending on the value of confinement ratio ξ.

Based on numerical studies, Tao *et al.* [45] proposed equations for determining f_B for both circular and rectangular CFST specimens. It is observed that f_B increases with increase in f_y or decrease in D/t, ratio where D is the steel column dimension and t is the thickness, and that the concrete cylinder compressive strength f_c' has no significant influence on the development of confining pressure at a later stage. But with increase in strength of concrete compressive strength leading to enhanced shrinkage, could delay the development of tube-to-concrete interaction and confining pressure in the column and thus, f_B decreases with an increase in f_c'. The following equations are proposed to obtain f_B:

$$f_B = \frac{(1+0.027f_y).e^{-0.02\frac{D}{t}}}{1+1.6e^{-10}.(f_c')^{4.8}} \quad \text{(circular CFST)} \tag{13}$$

$$f_B = \frac{0.25.(1+0.027f_y).e^{\frac{-0.02\sqrt{B^2+D^2}}{t}}}{1+1.6e^{-10}.(f_c')^{4.8}} \quad \text{(rectangular CFST)} \tag{14}$$

For the descending branch B to C as shown in Fig.19 the exponential function proposed by Binici [51] was used as:

$$\sigma = f_r + (f_c' - f_r)exp\left[-\left(\frac{\varepsilon-\varepsilon_{cc}}{\alpha}\right)^{\beta}\right] \qquad \varepsilon \geq \varepsilon_{cc} \tag{15}$$

where, f_r is the residual stress as shown in Fig.19; α and β are parameters that determine the shape of the softening portion B to C.

The expression for f_r is given as:

$$f_r = \begin{cases} 0.7\left(1-e^{-1.38\xi}\right)f_c' \leq 0.25f_c' & \text{(circular CFST)} \\ 0.1f_c', & \text{(rectangular CFST)} \end{cases} \tag{16}$$

The parameter α is mentioned in equation 3.17 is given as:

$$\alpha = \begin{cases} 0.04 - \frac{0.036}{1+e^{6.08\xi-3.49}} & \text{(circular CFST)} \\ 0.005 + 0.0075\xi & \text{(rectangular CFST)} \end{cases} \tag{17}$$

whereas β can be taken as 1.2 and 0.92 for circular and rectangular columns, respectively.

To consider the influence of concrete crushing on the elastic modulus of concrete, damage parameters were used in the CDP model to simulate the concrete behaviour more precisely. The compressive damage parameter corresponding to the inelastic strain is defined as the ratio of inelastic strain to the total strain capacity. The compressive damage values were applied via "suboptions" tool available in the CDP model. The predicted concrete compressive stress-strain curve and concrete damage parameter for a grade of C50 concrete from test [22] are displayed in Fig. 20 and Fig. 21.

3.3.3. Concrete tensile behaviour

The tensile behaviour of concrete under the influence of uniaxial tension can be modelled with the use of tension softening or tension stiffening behaviour. The tension softening behaviour can be obtained from the tensile stress vs. cracking displacement values, and the area under the curve is considered as fracture energy. Fracture energy is referred to as the energy required for a unit crack in the concrete. The tensile stress versus cracking displacement for concrete have been proposed by researchers in the past [43, 52, 53], and the most simplified form is the linear approximation to define the tensile cracking behaviour.

Even though the linear approximation for the tensile cracking behaviour can predict reasonably good results, the concrete response tends to be stiff and thus a smooth tension stiffening function of bi-linear approximation is proposed by Hillerborg and FIP [52, 53]. A linear and two bilinear tension softening models are presented in Fig.22. The bi-linear curves have a kink point and found to have been defined distinctively in [52] and [53]. The coordinates of the kink proposed by Hillerborg [52] are $(0.15f_t, 0.8\,G_f/f_t)$ and the coordinates proposed by FIP [53] are $(0.33f_t, 2\,G_f/f_t - 0.15w_{cr})$, where, w_{cr} is the crack opening displacement at the complete release of stress or fracture energy given as:

$$w_{cr} = \frac{\alpha_F G_F}{f_t} \tag{18}$$

where, α_F is a dimensionless coefficient that depends on the size of aggregate; G_F is the total fracture energy and f_t is the concrete uniaxial tensile strength. The value of α_F for 10 mm size aggregate is 7.75 as reported by Alfano *et al.* [54]. The uniaxial tensile strength of concrete f_t is obtained as per [55] given as $f_t = 0.56\sqrt{f_{cm}}$

As observed in Fig. 22, the tail of the bi-linear function proposed by CEB-FIP [53] is almost twice the length as that of the bi-linear function as proposed by Hillerborg [52], but the crack opening displacement will remain same at the kink point for both bilinear approximations.

The fracture energy G_F, as mentioned in Equation 18, has also been defined by various researchers and FIB model codes and the influence of each model is briefly presented here. The CEB-FIP Model Code 1993 [53] defines the fracture energy as the following equation:

$$G_F = G_{F0}(0.1\, f_{cm})^{0.7} \text{ (N/m)} \quad (19)$$

Trunk *et al.* [56] in 1998 proposed the fracture energy equation as:

$$G_F = a d_{max}^{n} \text{ (N/m), where, } a = 80.6 \text{ and } n = 0.32 \quad (20)$$

FIB Bulletin 42 (2008) [57] defines the fracture energy as:

$$G_F = G_{F0}\left(1 - \frac{7.7}{f_{cm}}\right) \quad (21)$$

The CEB-FIP Model Code 2010 [58] presented G_F as:

$$G_F = 73 \times f_{cm}^{0.18} \text{ (N/m)} \quad (22)$$

where, f_{cm} is the mean cylinder compressive strength in N/mm^2, given as $f_{cm} = f_{ck} + 8$; and f_{ck} is the characteristic cylinder compressive strength of concrete. The G_{F0}, which is a function of the maximum aggregate size is 26 N/m for aggregate size of 10 mm. For Equation 21, G_{F0} is a constant given as 180 N/m. The value of fracture energy from these four models are presented in Table 2 for concrete grade C50 as used in test [22], which shows that the energy predictions ranged from 88.99 N/m to 168.39 N/m, and therefore it is necessary to investigate its influence in tensile concrete behaviour of the bolted CFST connections.

The amount of fracture energy is the energy required for a unit crack in the concrete, the shape of the cracking displacement curve determines the rate at which the concrete loses its ability to bear the tensile stress. Thus, to consider the influence of concrete cracking, tensile damage parameters have been included in the numerical model and input made via “Suboption”

538 available in the CDP model in ABAQUS. The concrete tension damage can be fed in two ways,
539 either using strain or cracking displacement, and in this research programme the tensile damage
540 parameters were used with respect to cracking displacement as shown in Fig. 23.
541 For the investigation of influence of linear and two bilinear tensile softening models along with
542 four fracture energy values, an experimental model was adopted from [22], and the load-
543 displacement behaviour was calibrated with the experimental observation as presented in Fig.
544 24. From Fig. 24, it can be stated that, though the bolted connection behaviour with all the 12
545 models is similar with the experimental findings, there is delayed load drop and distinct
546 softening behaviour in case of linear (Fig. 24a) and CEB-FIP bilinear (Fig. 24b) models.
547 However, a better agreement was achieved with the Hillerborg's bilinear model (Fig. 24c).
548 Thus, the Hillerborg's bilinear model was able to accurately represent the concrete tensile
549 failure and using the Model Code 2010 fracture energy presented the most accurate behaviour
550 compared to the experimental counterpart. The tensile damage for the linear, CEB-FIP bilinear
551 and Hillerborg's bilinear tensile softening model using the Model Code 2010 fracture energy
552 is presented in Fig. 25. As observed for the tensile damage using CEB-FIP model (Fig. 25b),
553 the damage index captured is smaller than the other two approximations, this is because, full
554 tensile damage is defined at a higher cracking displacement for CEB-FIP bilinear model as
555 compared to the linear and Hillerborg's model (refer Fig. 22). It is to be noted that the elastic
556 modulus and Poisson's ratio of concrete were determined as $4700\sqrt{f_c'}$ as per [55] and 0.2 as
557 per [58] respectively.

558 **4. ABAQUS/Explicit solution**

559 As mentioned in the previous section, due to the complexities arising from many surface
560 interactions in the modelling of blind-bolted connection for CFST and open section beam, the
561 explicit scheme was adopted instead of the implicit. The basic difference between them is that
562 the implicit solution is unconditionally stable which is both an incremental and iterative scheme

and thus enforces equilibrium conditions. Whereas the explicit scheme is only incremental. In the implicit scheme, which uses the Newton Raphson method, the load is applied in increments and if the conditions of static equilibrium are not reached then it reduces the load increment, and this iteration continues until stability is achieved. Whereas the explicit scheme which uses the Euler's Central Difference method, keeps on applying the load increments even without satisfying equilibrium conditions. Due to the implicit scheme's iterative method, the analysis becomes more expensive as compared to the explicit scheme. In the current research scenario, numerical modelling with blind-bolts that consist of a number of bolt components interacting with end-plate, column tube and concrete core, complex contact problems could lead to convergence issues as a large number of iterations are needed to attain the stable condition. Therefore, the explicit scheme can be used for such complex problems and can overcome both convergence issues and reduce computational cost. But in an explicit scheme solution, certain issues like a large amount of time due to small increments and the inertia effect that are dominant, need to be carefully addressed.

The time increment or the time step in the explicit scheme is automatically determined by the solver and this time step is usually very small and may require large computational time. By increasing the time step in the explicit scheme, the total time required for the analysis can be reduced as this will lead to fewer increments and faster solution. This time step is dependent on the mesh size of the elements of the model, Young's modulus, and density of the material. The time step Δt can be represented as $\Delta t = \frac{L_e}{C}$, where $L_e$is the characteristic length of the element, which is defined as the smallest distance between two points of an element, and C is the speed of wave propagation, given as $C = \sqrt{\frac{E}{\rho}}$ where E is Young's modulus and ρ is material density; given as $\rho = \frac{m}{V}$, where m is the mass and V is the volume. Thus, to increase the time increment, either E may be reduced or ρ may be increased. The reduction of E is not practically

possible, but the density ρ can be increased by increasing the mass. This increase in mass is referred to as "mass scaling" and can be introduced in the system with a mass scaling factor (MSF). To measure the computational cost by use of the MSF, a comparison was studied using an EHB experimental model with and without the application of the MSF. Fig.26 presents the comparative response for the numerical model with and without the MSF, and it can observe that both the responses are identical. In Fig. 26, the computer CPU time required is also mentioned, which indicates that the model without MSF requires considerably more time as compared to the model with MSF, thus making the model without MSF more expensive.

The amplitude behaviour of the displacement-controlled loading applied to the connection is by default in the "linear step" or "tabular step" pattern. But as observed by Thai *et al.* [18], the use of "linear step" can result in some unwanted vibrations due to inertial dynamic effects during the elastic stage. On the other hand, using the "smooth step" amplitude the behaviour is smooth without any noise. Even though in the current study, no unwanted vibrations were generated by the use of the default "linear step", adopting the "smooth step" as load amplitude behaviour generates a better agreement in respect to the connection stiffness. Therefore, the "smooth step" amplitude is preferred over the "linear step". The load pattern and the comparative behaviour by use of linear and smooth steps are shown in Fig. 27 and Fig. 28, respectively.

Another way to reduce the computational time is by increasing the loading rate (LR). The applied LR should be such that it does not lead to the domination of inertia forces in the system as the kinetic energy (KE) within the model may mislead the numerical results. Therefore, it is necessary to keep the KE nearly zero as compared to the system internal energy (IE) to ensure that the inertia effect is not dominant or negligible. It is to be noted that, the selection of the LR is a trial-and-error method and for every LR considered, the corresponding KE to IE needs to be checked. The energy graph for various LR representing the corresponding KE and IE is

612 shown in Fig. 29, which shows that, as the LR is increased, the amount of KE also increases.
613 Therefore, small values of the LR should be selected, which also confirms the observation by
614 Thai *et al.* [18]. To further ensure that the dynamic explicit scheme is used appropriately, in
615 addition to the use of an appropriate mass scaling factor and a loading rate generating negligible
616 kinetic energy, the deformation behaviour may also be checked to ensure that the model has
617 been able to accurately replicate the experimental behaviour. A flow chart for determining the
618 appropriate MSF and LR is shown in Fig. 30.

619 Thus, if all the above-discussed points are implemented, the response of blind-bolted CFST
620 connection can be achieved or predicted with sufficient reliability and less computational time.
621 In the current study, the numerical models for HABB, EHB and SCBB connections with hollow
622 or CFST columns are generated and compared with their experimental counterparts. The
623 comparisons made are based on peak load, stiffness, post-yield behaviour, concrete tensile
624 damage, tube wall deformation and bolt elongation, which showed good agreement with the
625 experimental observations. The deformation behaviour and representative images of these
626 models are presented in Fig. 31 to Fig. 34 for comparison. Fig. 31 shows the concrete cone
627 developed due to the tensile pull-out of the anchored bolt for the experiment A-1M20-Mid [22],
628 being able to closely simulate by the FE analysis. Similarly, Fig. 32 shows the tube wall
629 deformation in experiment versus FE for the test A-1M20-Mid [22], where the tube had a
630 circular deformation of radius 100 mm. Fig. 33 shows the experiment versus FE of the bolt
631 shank fracture for the test EHB16-150-8.8D-C40-1 [24], along with no concrete damage. Fig.
632 34 presents experimental and FE comparison for the bolt hole deformation and tube wall
633 yielding for the specimen Oct-W150-T4-S [30].

634 **5. Conclusions**

635 A comprehensive numerical modelling technique for a blind-bolted CFST connection has been
636 discussed in this paper that aims to generate reliable FE models with enhanced computational
637 efficiency. Three different types of blind-bolts namely, the headed anchored blind-bolt
638 (HABB), the extended hollo-bolt (EHB) and the slip-critical blind-bolt (SCBB) having
639 connections with hollow or CFST columns were considered in this study, and the important
640 numerical modelling aspects have been discussed. The developed numerical models have also
641 been validated with their available counterpart experimental results with respect to load-
642 deformation behaviour , peak loads, and deformed geometry, which shows that the modelling
643 techniques adopted were sufficiently reliable. Following major conclusions can be drawn from
644 the present study.

645 (1) Making a simplified geometry of a complex blind-bolted connection can lead to generate
646 computationally efficient numerical models. Given that the blind-bolts are the smallest
647 components in the connection system, the numerical convergence is governed by the size of
648 bolt elements. Therefore, bolt element mesh size, that also controls the wave speed, needs to
649 be selected with proper judgement. Further, the bolt mesh size may influence the initial
650 stiffness if the global connection behaviour is controlled by the bolt component (weak bolt-
651 strong CFST).

652 (2) In EHB, the expandable sleeve is the tube bearing component, whereas in HABB and SCBB
653 the foldable washer and split-washer, respectively are the bearing components. The modelling
654 of the sleeve component in EHB and washers in HABB and SCBB is necessary to correctly
655 predict the connection behaviour .

656 (3) Ignoring the bolt pretension load significantly underestimate the strength and stiffness of
657 the bolted connection. The temperature load can be used to create bolt contraction that can

successfully replicate the bolt pretension load in the explicit analysis scheme. The bolt clamping length region can be used to apply the temperature load.

(4) The identification of the first-surface and second-surface in an interactive surface is not compulsory in an explicit solution scheme. The contact surfaces for HABB, EHB and SCBB bolts with CFST or hollow tube have been identified for reference in future studies.

(5) For correct representation of infilled concrete, the compressive and tensile damage parameters are required to be incorporated to capture the crushing or cracking of the core. Comparing three tension softening models with four different fracture energy models, it is observed that the use of Hillerborg's bilinear tensile damage model with fracture energy defined by *fib* Model Code 2010 gives the most reliable response for tensile pull-out loading.

(6) Applying Mass Scaling Factor (MSF) to increase the density of the smallest element is an effective way to increase the time-step for shorter computational time. Increased loading rate (LR) can be applied to further reduce the simulation time, but the selection of LR should be such that, the kinetic energy generated is negligible as compared to the system internal energy. This check will lead the dynamic explicit analysis to behave like a quasi-static analysis. A flow chart to determine MSF and LR is also presented.

(7) The techniques adopted can be used to achieve reliable behaviour of single and group bolt connections, that can not only lead to a better understanding of such connection behaviour , but also can help in making a rational design for future laboratory experiments.

Acknowledgement

The authors sincerely acknowledge the support from the Innovation and Technology Fund - Nano and Advanced Materials Institute (ITF-NAMI) for the project "Hong Kong Modular Integrated Construction (MiC) Innovations" (PolyU/ ZS12) and from the Chinese National

Engineering Research Centre for Steel Construction (Hong Kong Branch) at The Hong Kong Polytechnic University.

References

[1] J. Zhu, T. Chan, Experimental investigation on octagonal concrete filled steel stub columns under uniaxial compression, Journal of Constructional Steel Research 147 (2018) 457-467.

[2] J.-Y. Zhu, T.-M. Chan, Behaviour of polygonal-shaped steel-tube columns filled with high-strength concrete, Proceedings of the Institution of Civil Engineers - Structures and Buildings 171(2) (2018) 96-112.

[3] J. Chen, T.-M. Chan, K.-F. Chung, Design of square and rectangular CFST cross-sectional capacities in compression, Journal of Constructional Steel Research 176 (2021) 106419.

[4] J.-Y. Zhu, T.-M. Chan, Experimental investigation on steel-tube-confined-concrete stub column with different cross-section shapes under uniaxial-compression, Journal of Constructional Steel Research 162 (2019) 105729.

[5] H. Fang, T.-M. Chan, B. Young, Structural performance of concrete-filled cold-formed high-strength steel octagonal tubular stub columns, Engineering Structures 239 (2021) 112360.

[6] J. Jiang, J. Zhang, J. Liu, S.P. Chiew, C.K. Lee, Effect of welding and heat treatment on strength of high-strength steel columns, Journal of Constructional Steel Research 151 (2018) 238-252.

[7] A.W. Lacey, W. Chen, H. Hao, K. Bi, Review of bolted inter-module connections in modular steel buildings, Journal of Building Engineering 23 (2019) 207-219.

[8] E.-F. Deng, L. Zong, Y. Ding, Z. Zhang, J.-F. Zhang, F.-W. Shi, L.-M. Cai, S.-C. Gao, Seismic performance of mid-to-high rise modular steel construction - A critical review, Thin-Walled Structures 155 (2020) 106924.

[9] J.-F. Wang, L.-H. Han, B. Uy, Behaviour of flush end plate joints to concrete-filled steel tubular columns, Journal of Constructional Steel Research 65(4) (2009) 925-939.

706 [10] J. Wang, L. Chen, Experimental investigation of extended end plate joints to concrete-
707 filled steel tubular columns, Journal of Constructional Steel Research 79 (2012) 56-70.
708 [11] H.-T. Thai, B. Uy, Yamesri, F. Aslani, Behaviour of bolted endplate composite joints to
709 square and circular CFST columns, Journal of Constructional Steel Research 131 (2017) 68-
710 82.
711 [12] Z. Tao, W. Li, B.-L. Shi, L.-H. Han, Behaviour of bolted end-plate connections to
712 concrete-filled steel columns, Journal of Constructional Steel Research 134 (2017) 194-208.
713 [13] H. Agheshlui, H. Goldsworthy, E. Gad, H. Yao, Tensile Behavior of Groups of Anchored
714 Blind Bolts within Concrete-Filled Steel Square Hollow Sections, Journal of Structural
715 Engineering 142(2) (2016) 04015125.
716 [14] ABAQUS, Dassault Systems, Waltham, MA, USA, 2019.
717 [15] J. Wang, B.F. Spencer, Experimental and analytical behavior of blind bolted moment
718 connections, Journal of Constructional Steel Research 82 (2013) 33-47.
719 [16] W. Tizani, A. Al-Mughairi, J.S. Owen, T. Pitrakkos, Rotational stiffness of a blind-bolted
720 connection to concrete-filled tubes using modified Hollo-bolt, Journal of Constructional Steel
721 Research 80 (2013) 317-331.
722 [17] Y. Oktavianus, H.M. Goldsworthy, E. Gad, Group Behavior of Double-Headed Anchored
723 Blind Bolts within Concrete-Filled Circular Hollow Sections under Cyclic Loading, Journal of
724 Structural Engineering 143(10) (2017).
725 [18] H.-T. Thai, T.P. Vo, T.-K. Nguyen, C.H. Pham, Explicit simulation of bolted endplate
726 composite beam-to-CFST column connections, Thin-Walled Structures 119 (2017) 749-759.
727 [19] T. Pokharel, H.M. Goldsworthy, E.F. Gad, Tensile behaviour of double headed anchored
728 blind bolt in concrete filled square hollow section under cyclic loading, Construction and
729 Building Materials 200 (2019) 146-158.

730 [20] ONESIDE Brochure B-N012 Data Sheet, AJAX Engineered Fasteners Victoria, Australia,
731 2002.
732 [21] Y. Oktavianus, H. Yao, H.M. Goldsworthy, E.F. Gad, Pull-out behaviour of blind bolts
733 from concrete-filled tubes, Proceedings of the Institution of Civil Engineers - Structures and
734 Buildings 168(10) (2015) 747-759.
735 [22] H. Agheshlui, H. Goldsworthy, E. Gad, S. Fernando, Tensile behaviour of anchored blind
736 bolts in concrete filled square hollow sections, Materials and Structures 49(4) (2016) 1511-
737 1525.
738 [23] The Original Expansion Bolt for Structural Steel, in: L. International (Ed.) Bradford,
739 England, 2013.
740 [24] T. Pitrakkos, W. Tizani, Experimental behaviour of a novel anchored blind-bolt in tension,
741 Engineering Structures 49 (2013) 905-919.
742 [25] W. Tizani, T. Pitrakkos, Performance of T-Stub to CFT Joints Using Blind Bolts with
743 Headed Anchors, Journal of Structural Engineering 141(10) (2015) 04015001.
744 [26] W. Tizani, M. Mahmood, D. Bournas, Effect of Concrete Infill and Slenderness on
745 Column-Face Component in Anchored Blind-Bolt Connections, Journal of Structural
746 Engineering 146(4) (2020) 04020041.
747 [27] P.P. Debnath, T.-M. Chan, Tensile behaviour of headed anchored hollo-bolts in concrete
748 filled hollow steel tube connections, Engineering Structures 234 (2021) 111982.
749 [28] W. Wang, M. Li, Y. Chen, X. Jian, Cyclic behavior of endplate connections to tubular
750 columns with novel slip-critical blind bolts, Engineering Structures 148 (2017) 949-962.
751 [29] W. Wang, L. Li, D. Chen, Progressive collapse behaviour of endplate connections to cold-
752 formed tubular column with novel Slip-Critical Blind Bolts, Thin-Walled Structures 131
753 (2018) 404-416.

754 [30] F. Xu, T.-M. Chan, Structural Behaviour of Blind-Bolted T-stub to Octagonal Tube
755 Connections Using Normal and High Strength Steels, Ninth International Conference on
756 Advances in Steel Structures (ICASS), Hong Kong, 2018, pp. 1510-1520.
757 [31] CEN. Eurocode 3 : Design of Steel Structures- Part 1-8: Design of Joints. BS EN 1993-1-
758 8: 2005, in: B.S. Institution (Ed.) 2005.
759 [32] X. Dai, D. Lam, Numerical modelling of the axial compressive behaviour of short
760 concrete-filled elliptical steel columns, Journal of Constructional Steel Research 66(7) (2010)
761 931-942.
762 [33] H. Shakir-Khalil, Pushout strength of concrete-filled steel hollow - sections, The
763 Structural Engineer 71(13) (1993) 230-243.
764 [34] X. Qu, Z. Chen, D. Nethercot, L. Gardner, M. Theofanous, Push-out tests and bond
765 strength of rectangular CFST columns, Steel & Composite Structures 19(1) (2015) 21-41.
766 [35] X. Yun, L. Gardner, Stress-strain curves for hot-rolled steels, Journal of Constructional
767 Steel Research 133 (2017) 36-46.
768 [36] Q.Q. Liang, Performance-based analysis of concrete-filled steel tubular beam–columns,
769 Part I: Theory and algorithms, Journal of Constructional Steel Research 65(2) (2009) 363-372.
770 [37] Z. Tao, X.-Q. Wang, B. Uy, Stress-Strain Curves of Structural and Reinforcing Steels after
771 Exposure to Elevated Temperatures, Journal of Materials in Civil Engineering 25(9) (2013)
772 1306-1316.
773 [38] EN 1993-1-1 (2005): Eurocode 3: Design of steel structures - Part 1-1: General rules and
774 rules for buildings, 2005.
775 [39] T. Yu, J.G. Teng, Y.L. Wong, S.L. Dong, Finite element modeling of confined concrete-
776 I: Drucker–Prager type plasticity model, Engineering Structures 32(3) (2010) 665-679.

[40] A. Earij, G. Alfano, K. Cashell, X. Zhou, Nonlinear three–dimensional finite–element modelling of reinforced–concrete beams: Computational challenges and experimental validation, Engineering Failure Analysis 82 (2017) 92-115.

[41] J. Lubliner, J. Oliver, S. Oller, E. Oñate, A plastic-damage model for concrete, International Journal of Solids and Structures 25(3) (1989) 299-326.

[42] J. Lee, G.L. Fenves, Plastic-Damage Model for Cyclic Loading of Concrete Structures, Journal of Engineering Mechanics 124(8) (1998) 892-900.

[43] ABAQUS 6.14, CAE User's Guide, Dassault Systemes, 2014.

[44] J. Lee, L. Fenves Gregory, Plastic-Damage Model for Cyclic Loading of Concrete Structures, Journal of Engineering Mechanics 124(8) (1998) 892-900.

[45] Z. Tao, Z.-B. Wang, Q. Yu, Finite element modelling of concrete-filled steel stub columns under axial compression, Journal of Constructional Steel Research 89 (2013) 121-131.

[46] L.-H. Han, G.-H. Yao, Z. Tao, Performance of concrete-filled thin-walled steel tubes under pure torsion, Thin-Walled Structures 45(1) (2007) 24-36.

[47] Q.Q. Liang, S. Fragomeni, Nonlinear analysis of circular concrete-filled steel tubular short columns under axial loading, Journal of Constructional Steel Research 65(12) (2009) 2186-2196.

[48] H.-T. Hu, C.-S. Huang, M.-H. Wu, Y.-M. Wu, Nonlinear Analysis of Axially Loaded Concrete-Filled Tube Columns with Confinement Effect, Journal of Structural Engineering 129(10) (2003) 1322-1329.

[49] A.K. Samani, M.M. Attard, A stress–strain model for uniaxial and confined concrete under compression, Engineering Structures 41 (2012) 335-349.

[50] B. De Nicolo, L. Pani, E. Pozzo, Strain of concrete at peak compressive stress for a wide range of compressive strengths, Materials and Structures 27(4) (1994) 206-210.

801 [51] B. Binici, An analytical model for stress–strain behavior of confined concrete, Engineering
802 Structures 27(7) (2005) 1040-1051.
803 [52] A. Hillerborg, The theoretical basis of a method to determine the fracture energyGFof
804 concrete, Materials and Structures 18(4) (1985) 291-296.
805 [53] M. CEB-FIP, 90, Design of concrete structures. CEB-FIP Model Code 1990, British
806 Standard Institution, London (1993).
807 [54] G. Alfano, P.D. Fiorenzo De Cicco, A. Prota, Intermediate Debonding Failure of RC
808 Beams Retrofitted in Flexure with FRP: Experimental Results versus Prediction of Codes of
809 Practice, Journal of Composites for Construction 16(2) (2012) 185-195.
810 [55] Committee 318, Building Code Requirements for Structural Concrete (ACI 318-11) and
811 Commentary (ACI 318R-11), ACI (American Concrete Institute)
812 ACI, Farmington Hills, MI, 2011.
813 [56] B. Trunk, F. Wittmann, Experimental investigation into the size dependence of fracture
814 mechanics parameters. , Proceedings of Third International Conference of Fracture Mechanics
815 of Concrete Structures, 1998, pp. 1937-1948.
816 [57] Constitutive modelling for high strength/high performance concrete- fib Bulletin 42,
817 Lausanne, Switzerland, 2008.
818 [58] FIP, CEB-FIP Model Code 2010-Final draft, International Federation for Structural
819 Concrete, 2010.
820
821

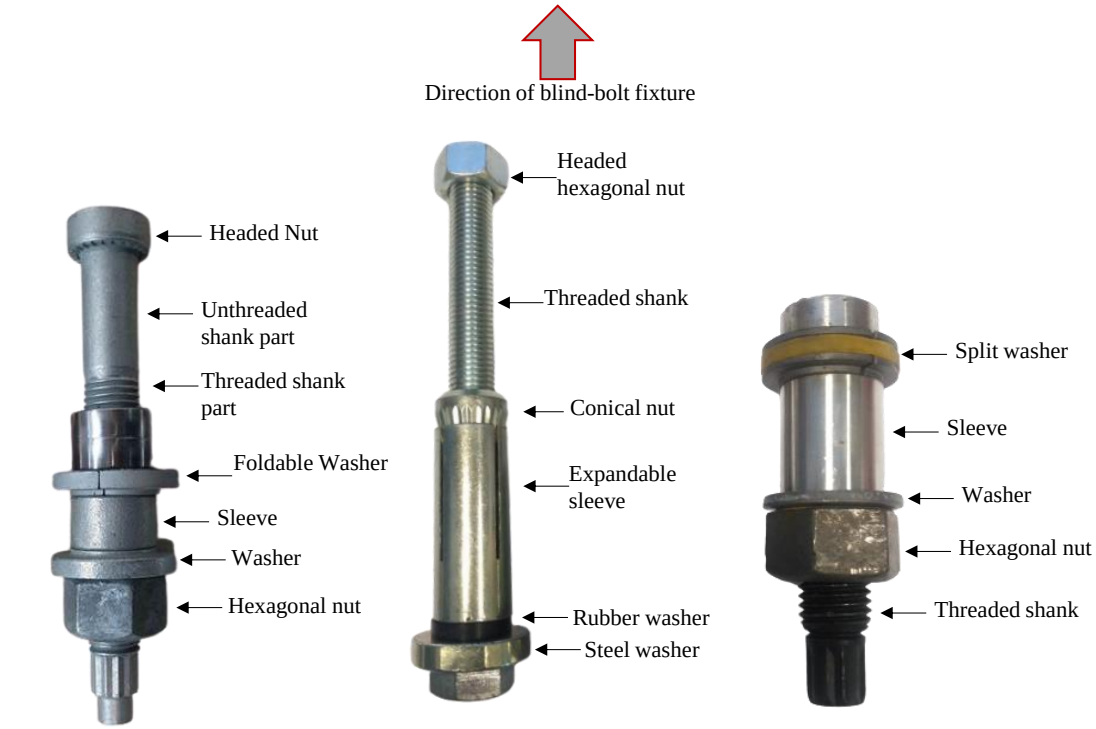

(a) Headed anchored blind-bolt (HABB)

(b) Extended hollo bolt (EHB)

(c) Slip-critical blind-bolt (SCBB)

Fig. 1. Types of blind bolts considered in the study.

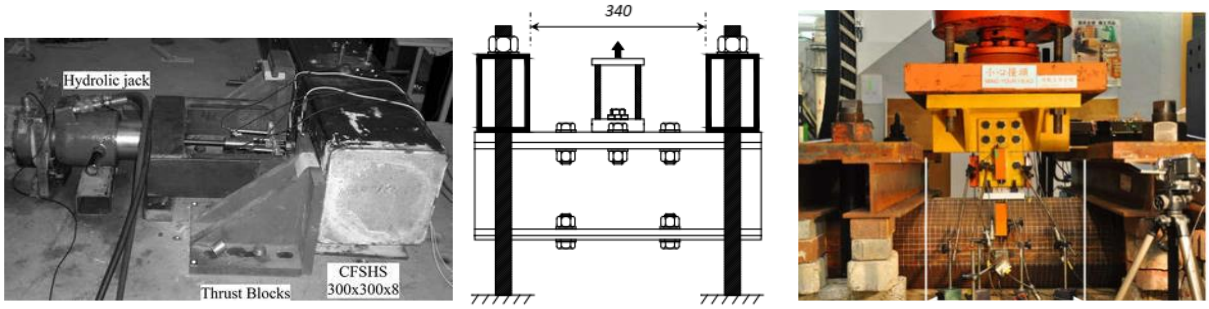

(a) HABB-CFST connection [22]

(b) EHB-CFST connection [24]

(c) SCBB-hollow tube connection [30]

Fig. 2. Experimental setup for bolt pull-out tests using different types of blind-bolts.

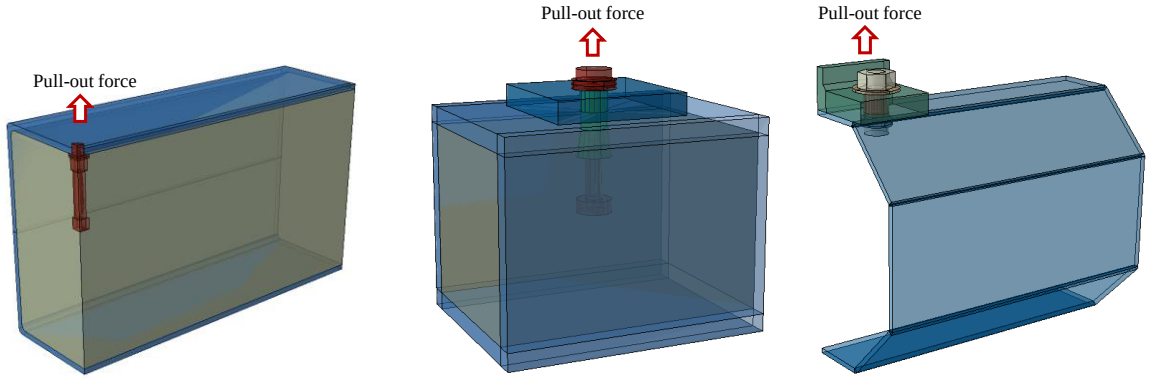

(a) Numerical model of HABB-CFST connection for test by [22]

(b) Numerical model of EHB-CFST connection for test by [24]

(c) Numerical model of SCBB-hollow tube connection for test by [30]

Fig. 3. Simplified numerical models for bolt pull-out tests using different types of blind-bolts.

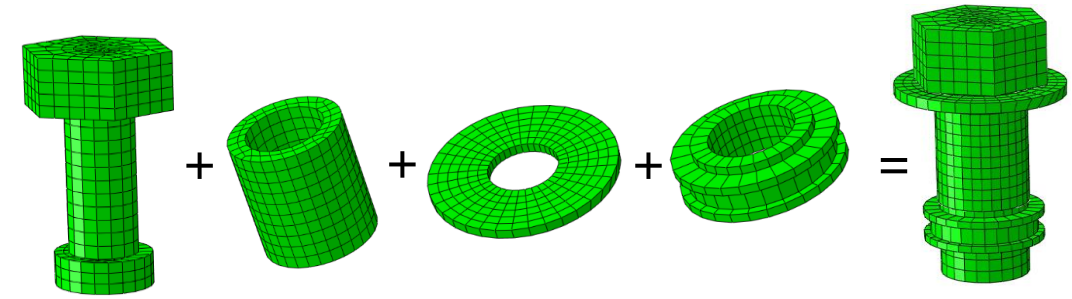

Fig. 4. FE models of SCBB in parts and full assembly.

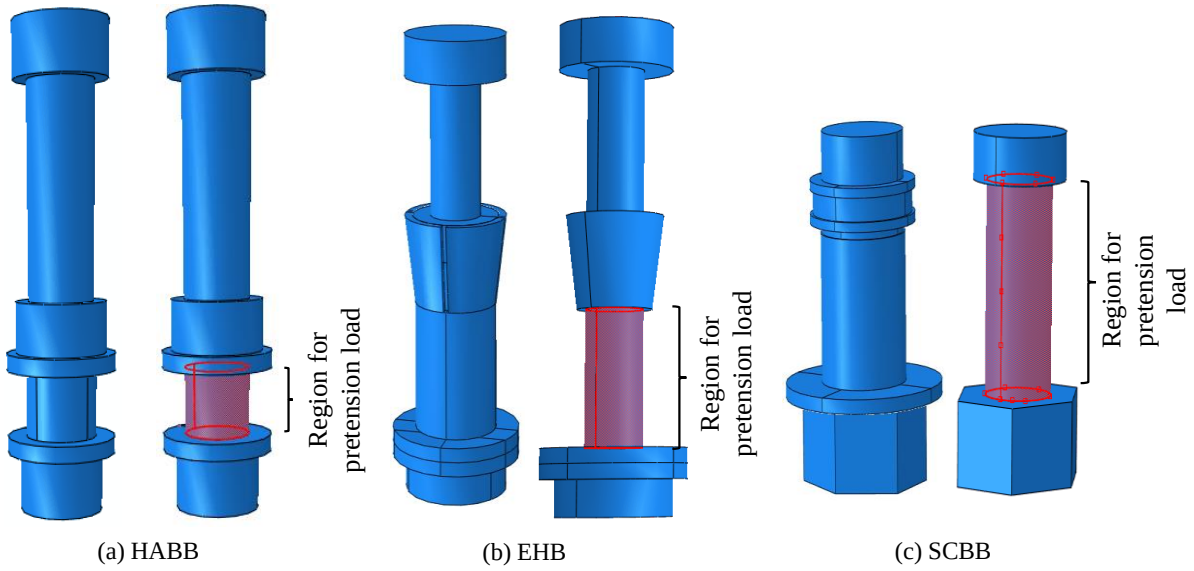

Fig. 5. FE models of blind-bolts and region for applying preload after removal of sleeve.

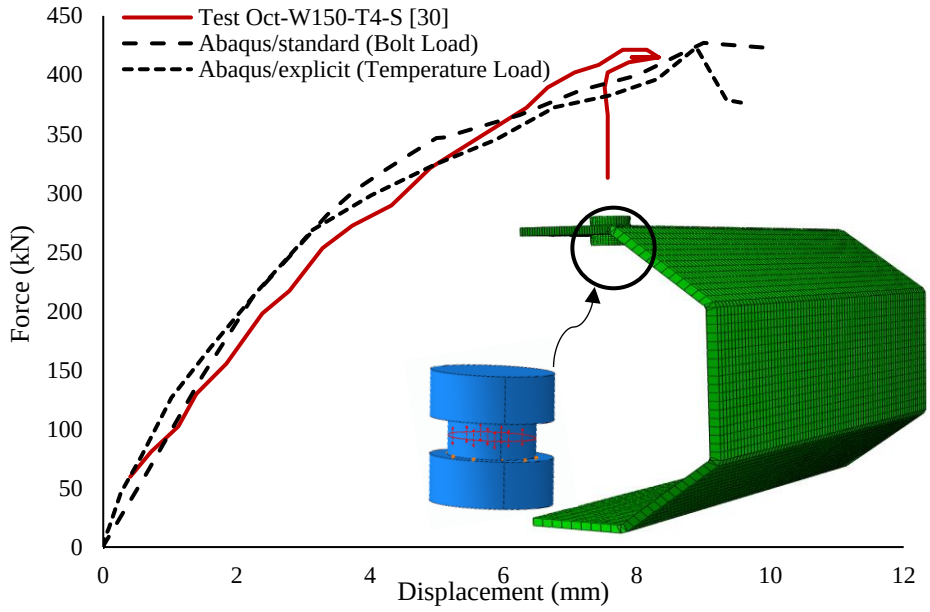

Fig. 6. Comparison of Abaqus/standard and Abaqus/Explicit analysis using a simplified model.

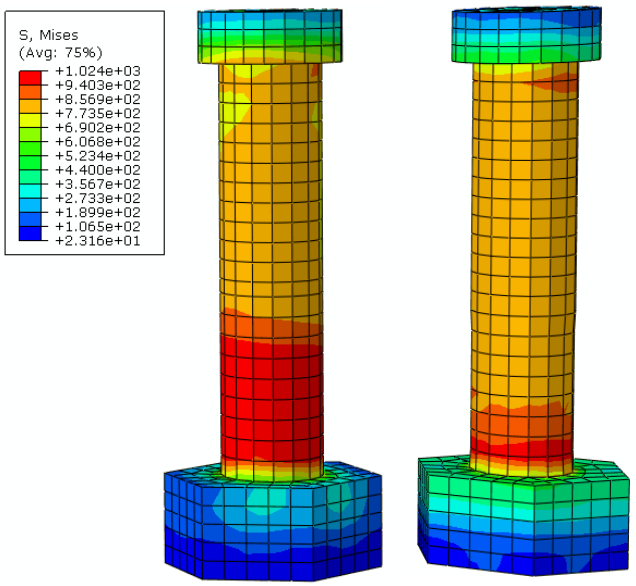

(a) Bolt load (in Abaqus/Standard)

(b) Temperature load (Abaqus/Explicit)

Fig. 7. Comparison between bolt stresses due to pretension by standard and explicit solver.

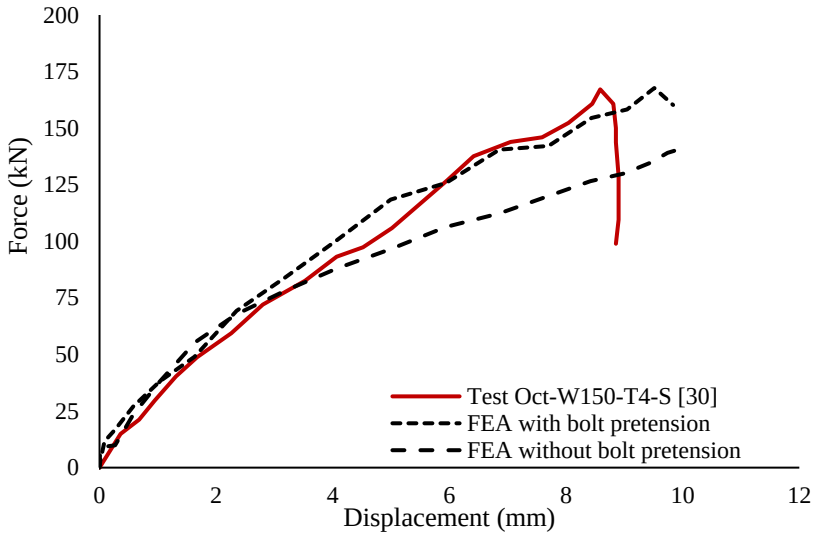

Fig. 8. Comparison with and without applying bolt pretension force.

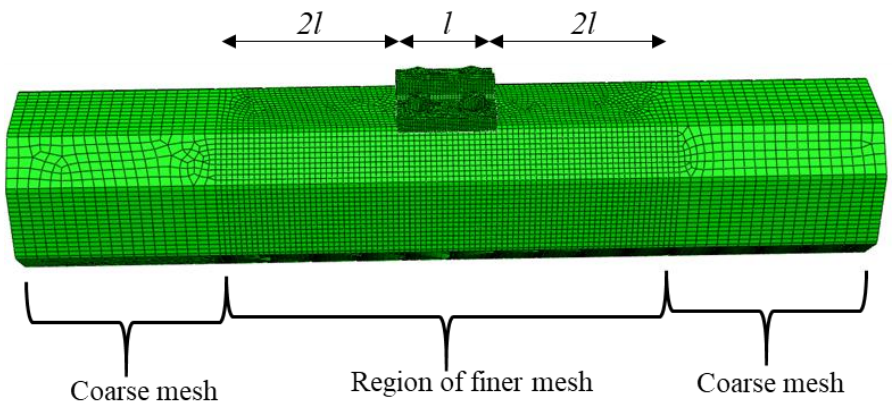

Fig. 9. Mesh size distribution for SCBB connection for the test [30].

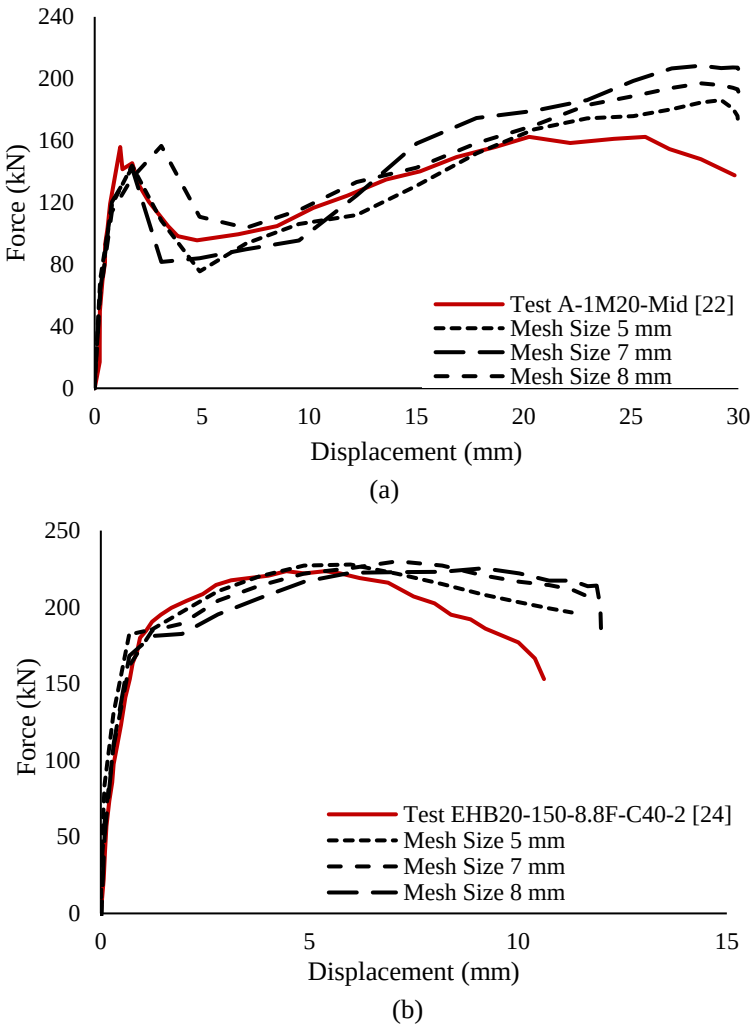

Fig. 10. Influence of bolt mesh size for FE studies compared with tests.

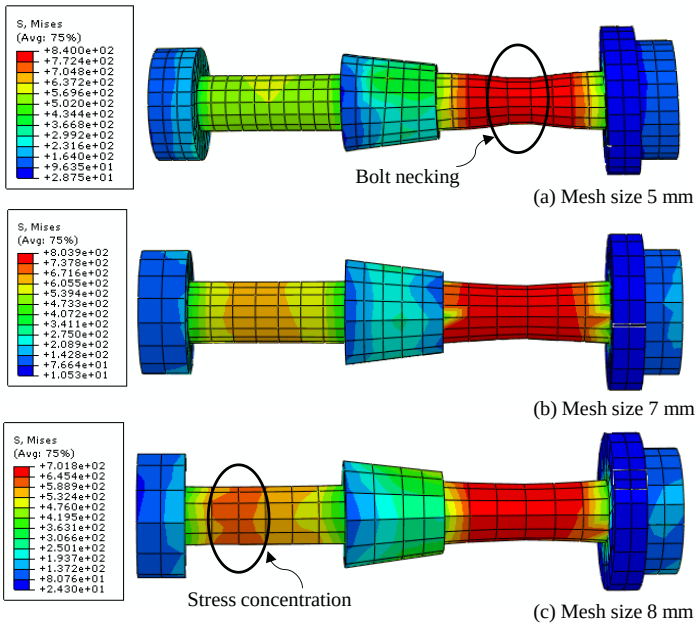

Fig. 11. Stresses in bolt with varied bolt mesh size.

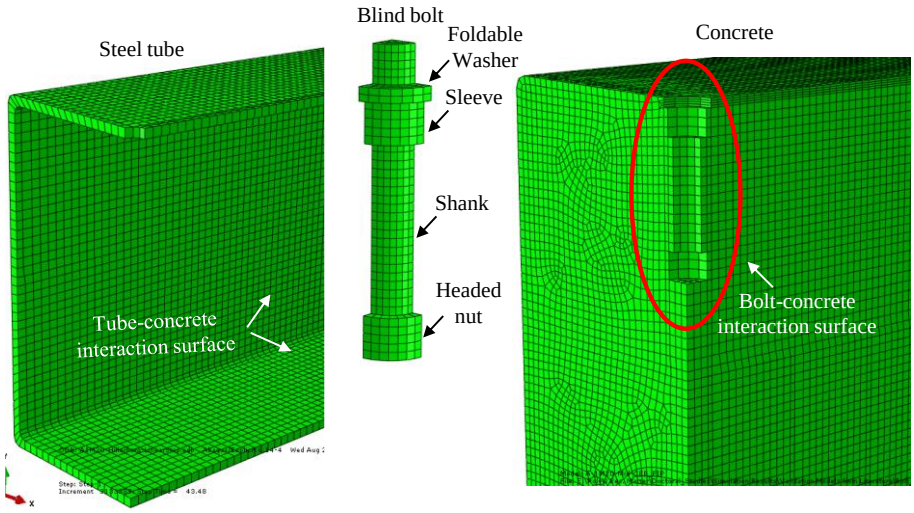

(a) Interaction surfaces in HABB-CFST tube connection for the test [22].

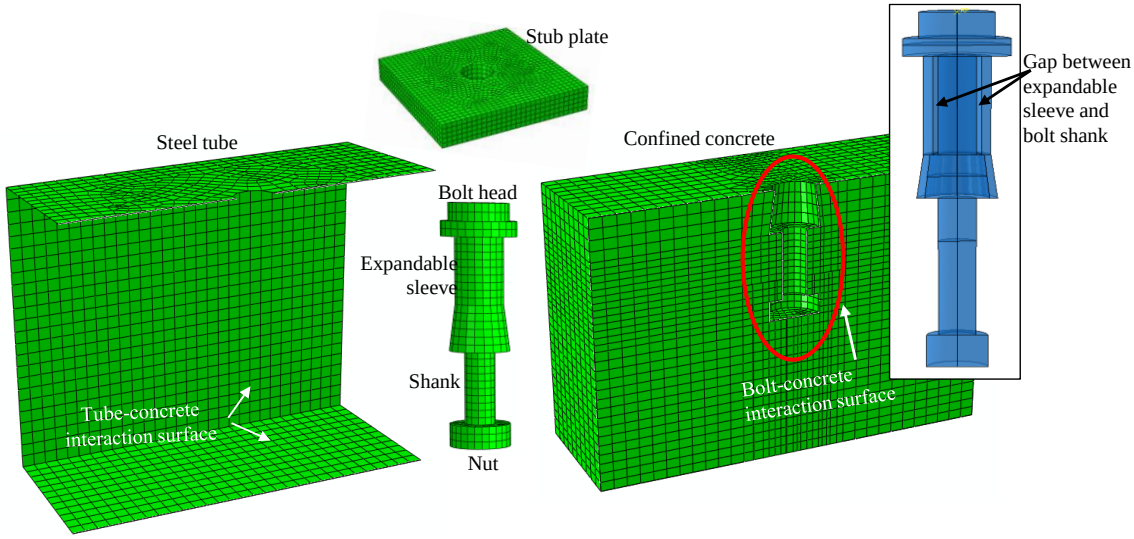

(b) Interaction surfaces in EHB-CFST connection for the test [24].

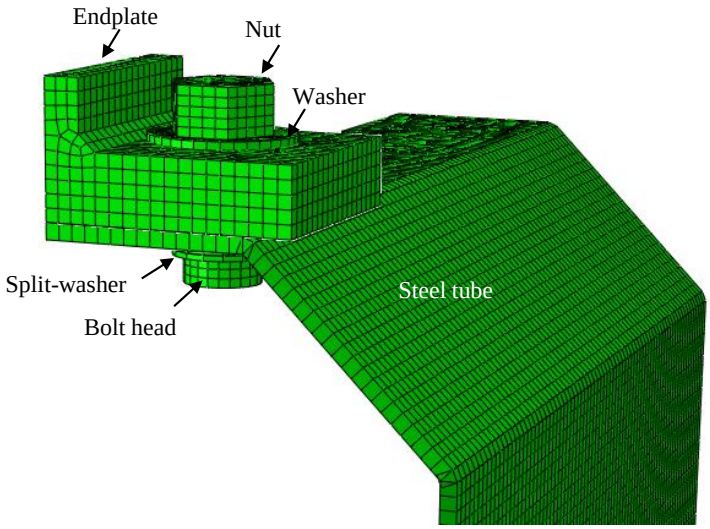

(c) Interaction surfaces in SCBB and hollow tube connection for the test [30].

Fig. 12. Contact surfaces in various bolted connection.

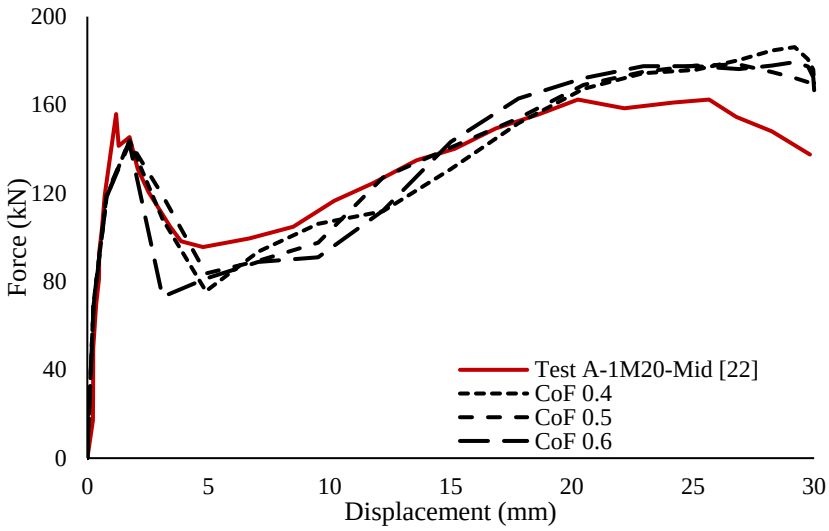

Fig. 13. Influence of friction coefficient between steel and concrete.

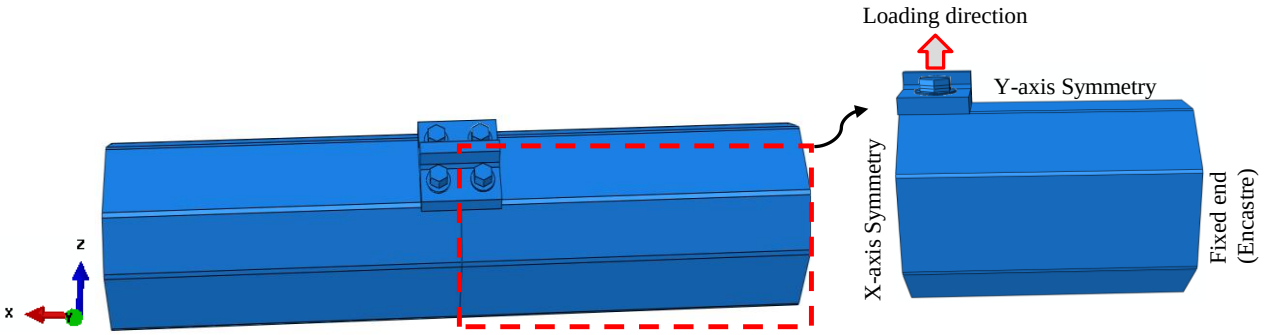

(a) Full model (CPU time: 10.58 hrs.) (b) Quarter model (CPU time: 1.85 hrs.)

Fig.14. FE full and quarter model of Oct-W150-T4-S [30].

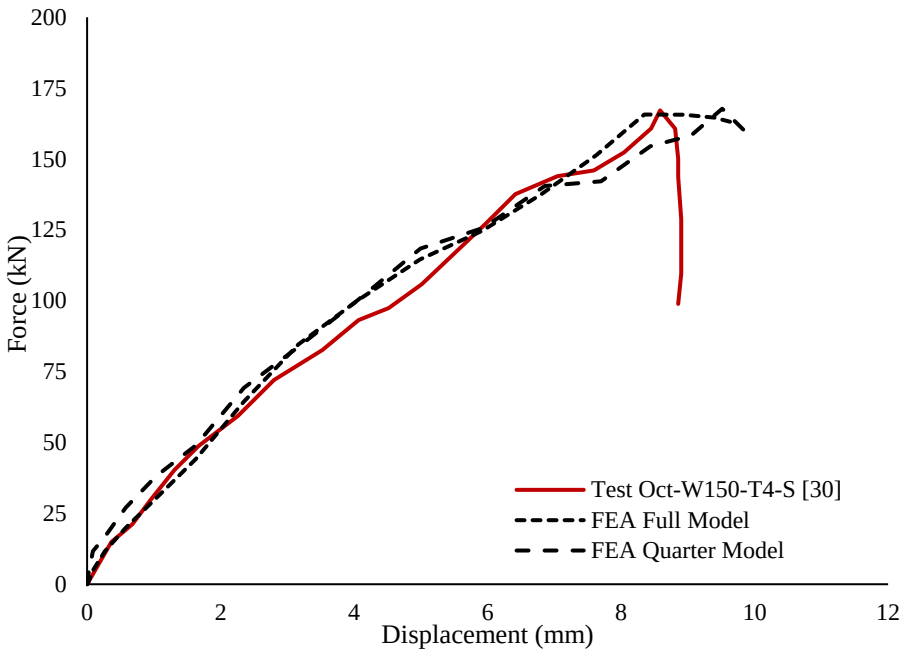

Fig. 15. Comparison of full and quarter model for the test [30].

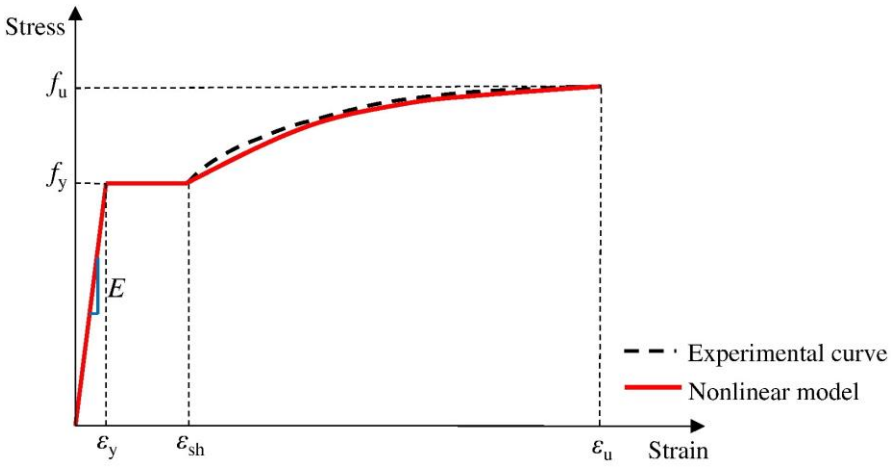

Fig. 16. Steel bilinear plus nonlinear hardening model as per [35].

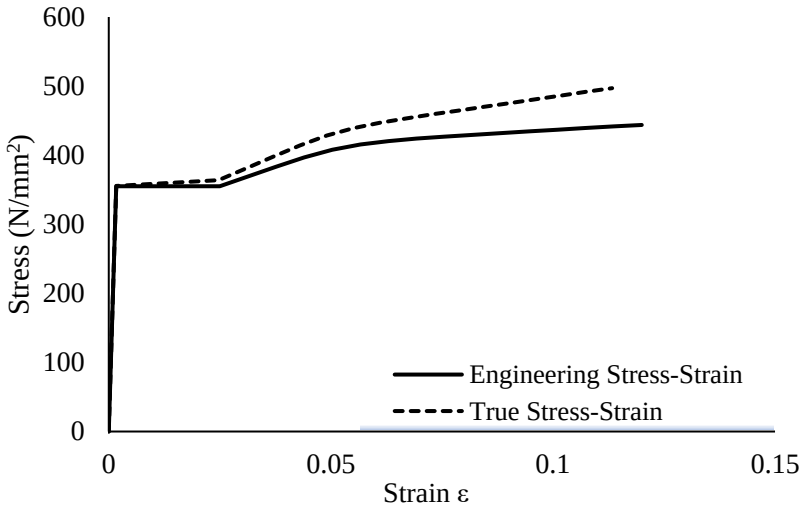

Fig. 17. Stress-strain curve adopted for constitutive modelling of steel tube.

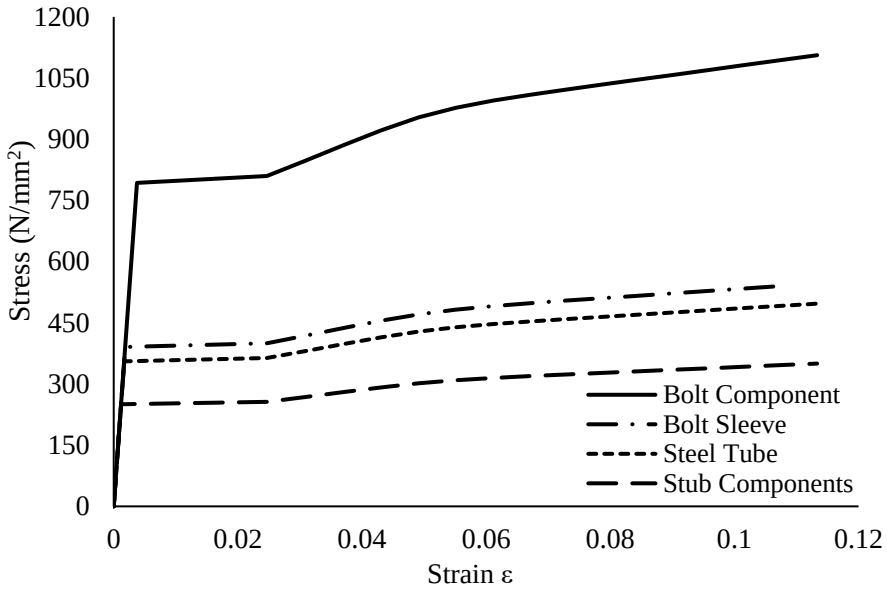

Fig. 18. Representative stress-strain plots for different steel components.

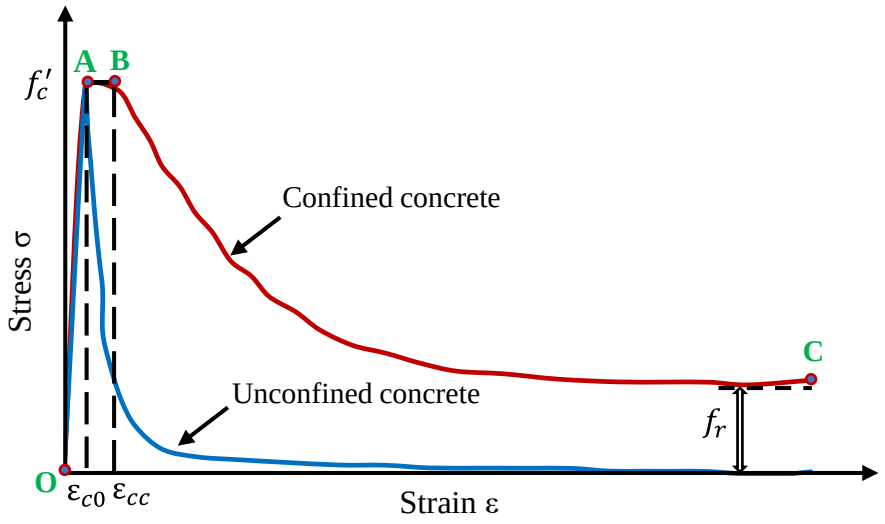

Fig. 19. Stress-strain model for unconfined and confined concrete adapted from [45].

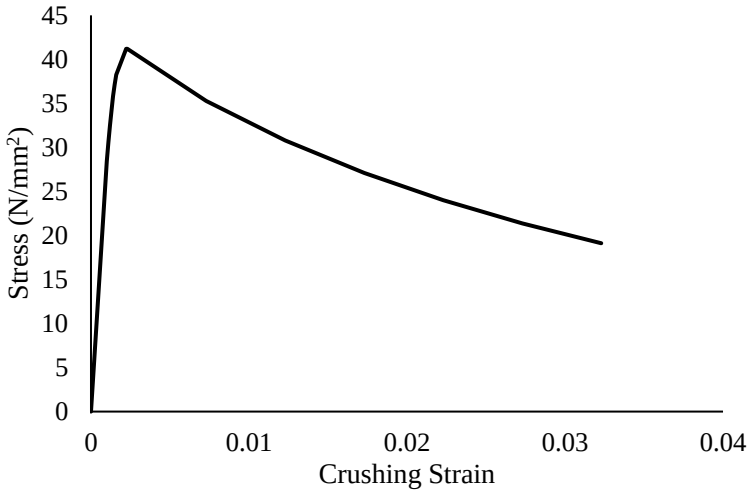

Fig. 20. Compressive stress vs strain curve for confined concrete.

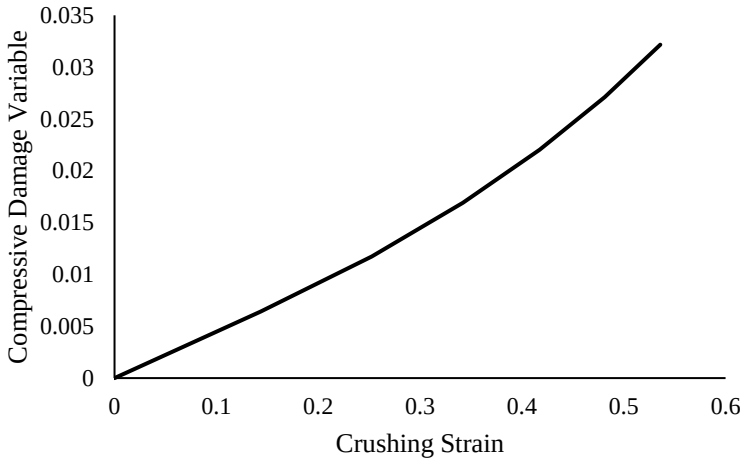

Fig. 21. Concrete compressive damage evolution.

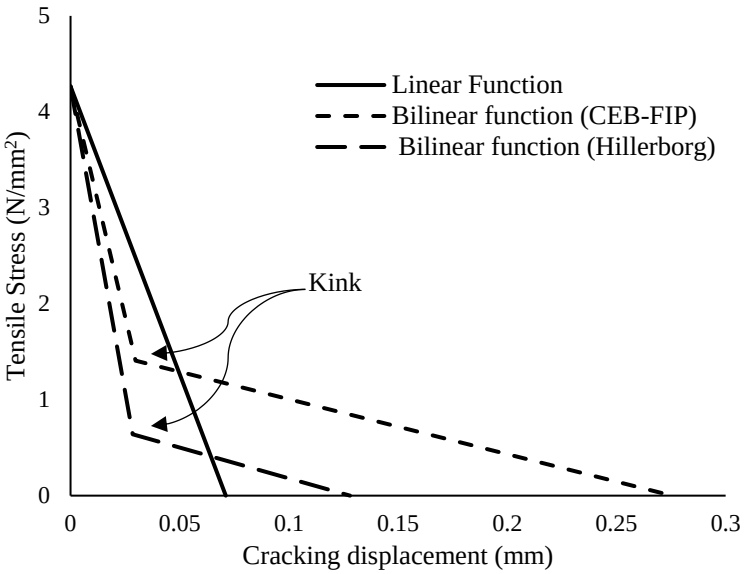

Fig. 22. Tension softening models.

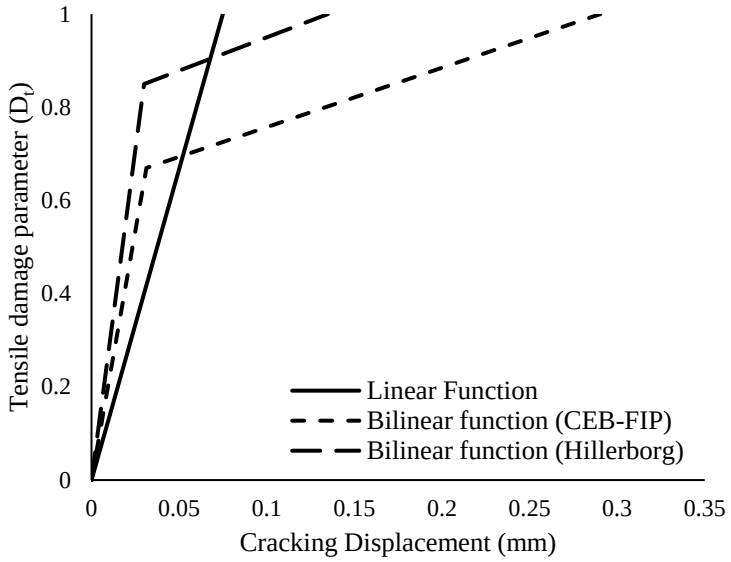

Fig. 23. Concrete tensile damage evolution.

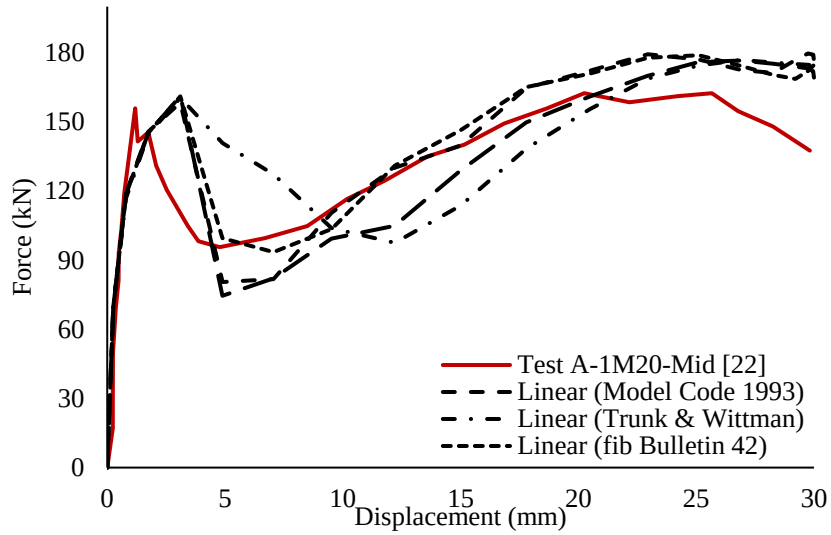

(a) Influence of fracture energy models using linear tensile damage.

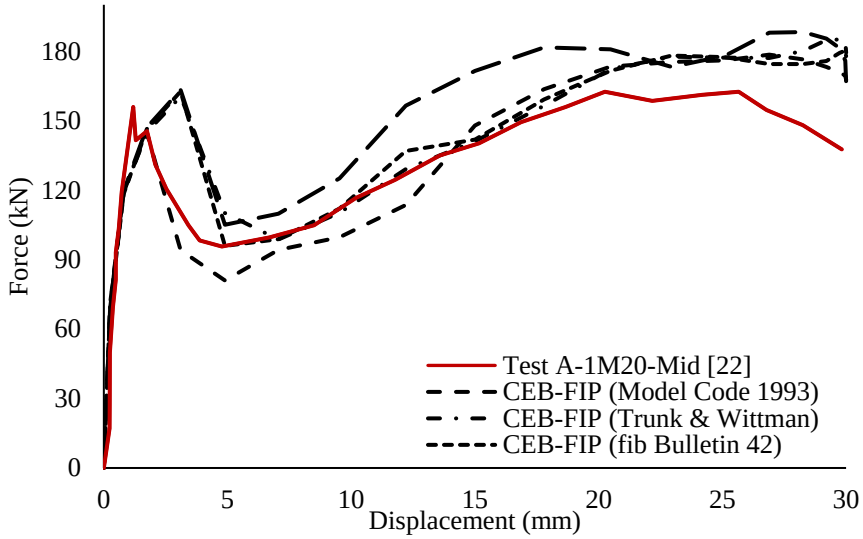

(b) Influence of fracture energy models using bilinear CEB-FIP damage.

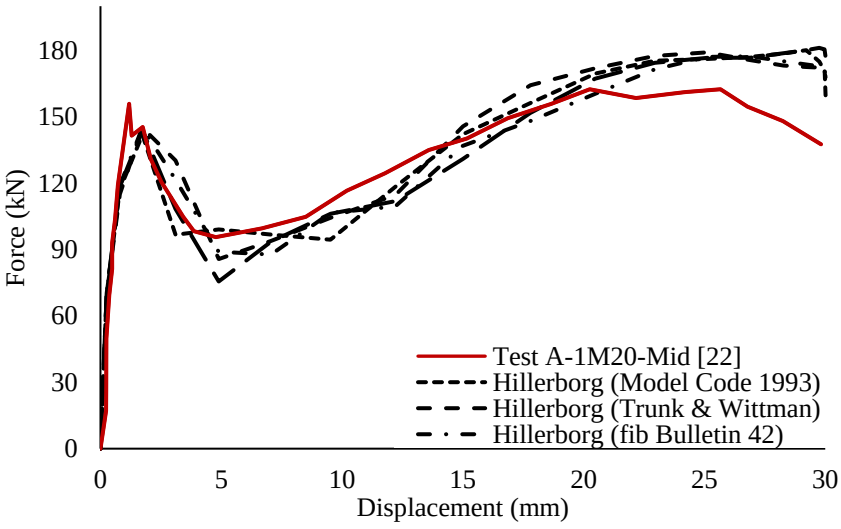

(c) Influence of fracture energy models using bilinear Hillerborg's tensile damage.

Fig. 24. Behavior of specimen A-1M20-Mid [22] with damage models in with various fracture energy.

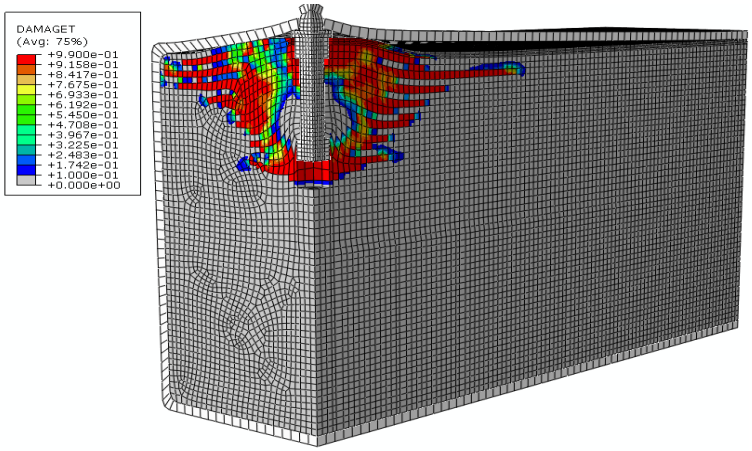

(a) Tensile damage with linear model

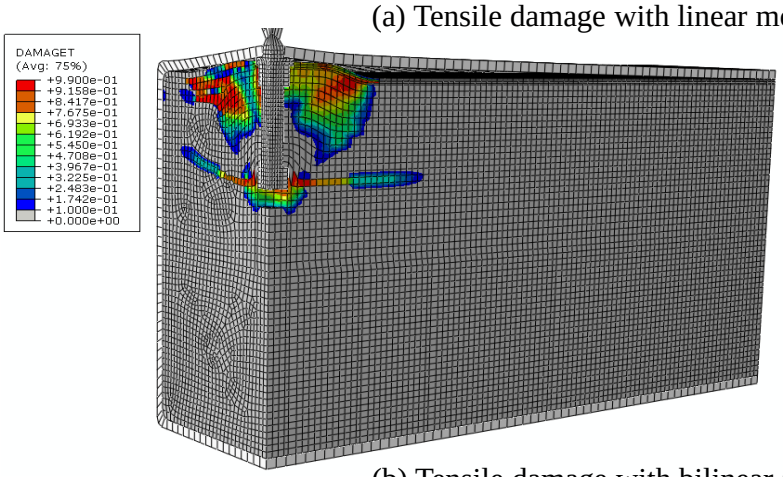

(b) Tensile damage with bilinear CEB-FIP model

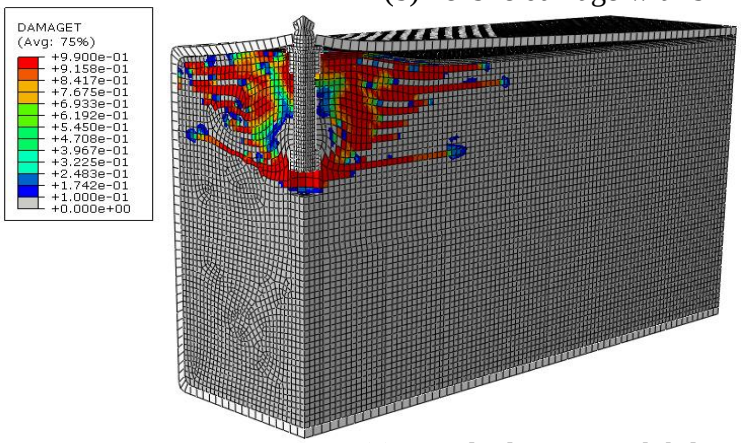

(c) Tensile damage with bilinear Hillerborg's model

Fig. 25. Concrete tensile damage of specimen A-1M20-Mid [22] with various damage models using fracture energy of CEB-FIP Model Code 2010.

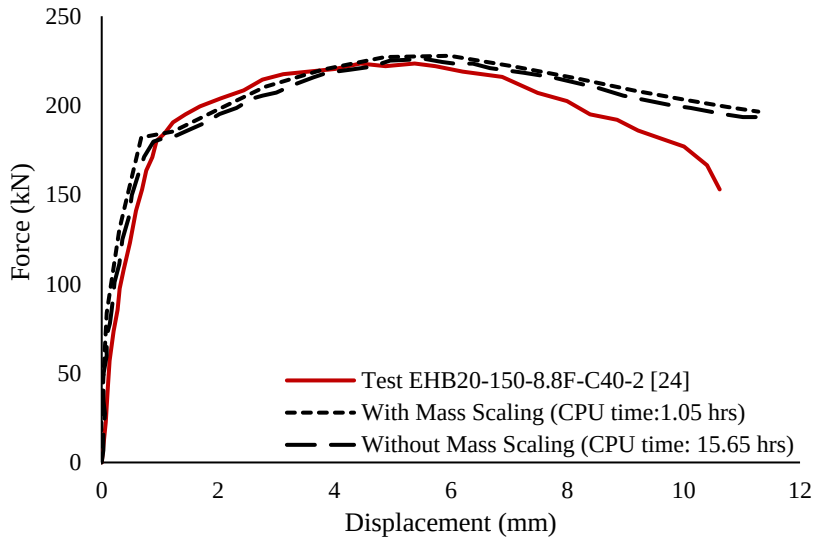

Fig. 26. Comparison with and without the use of mass scaling in the explicit solver.

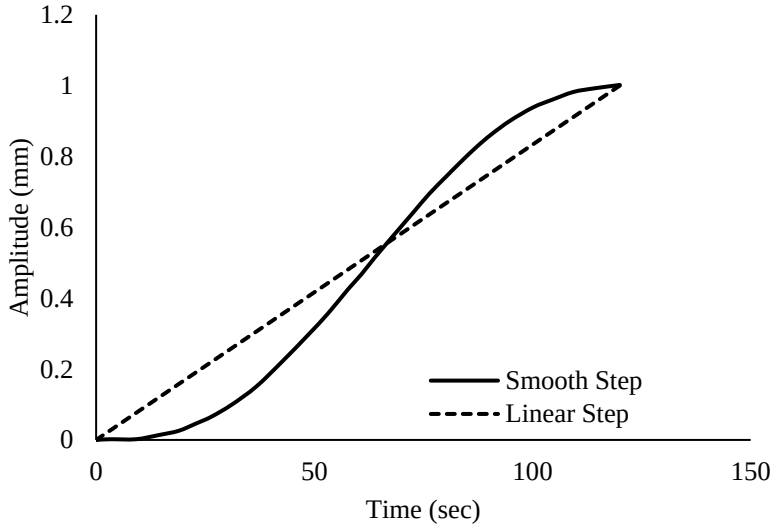

Fig. 27. Comparison of linear step and smooth step for defining amplitude.

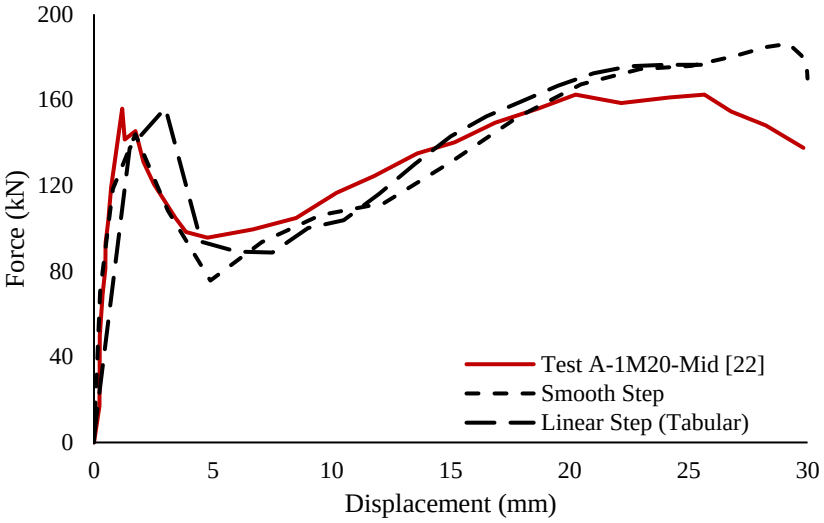

Fig. 28. Influence of linear step and smooth step in FE analysis.

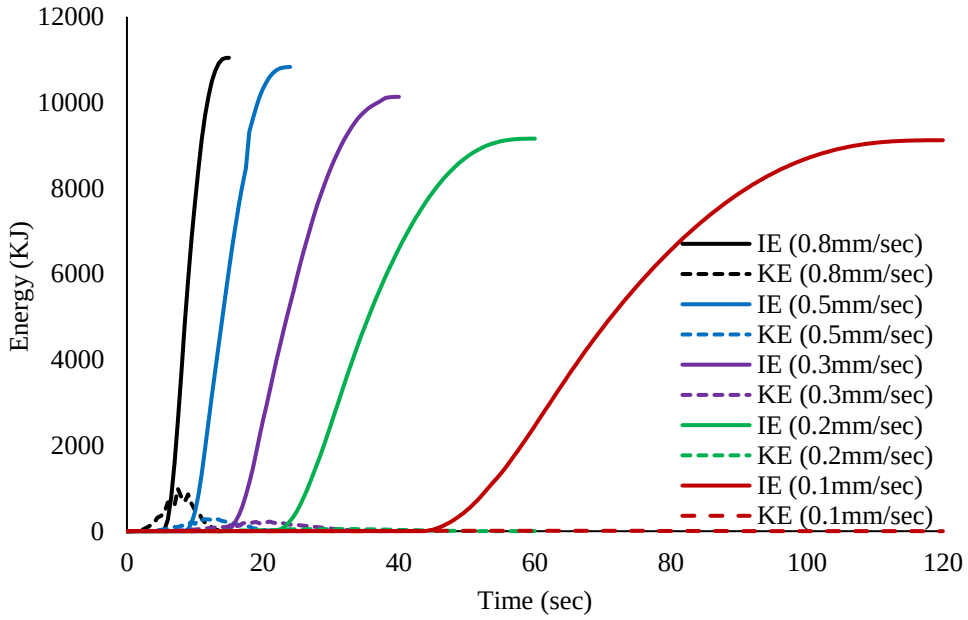

Fig. 29. Comparison of kinetic and internal energy with the use of various loading rate.

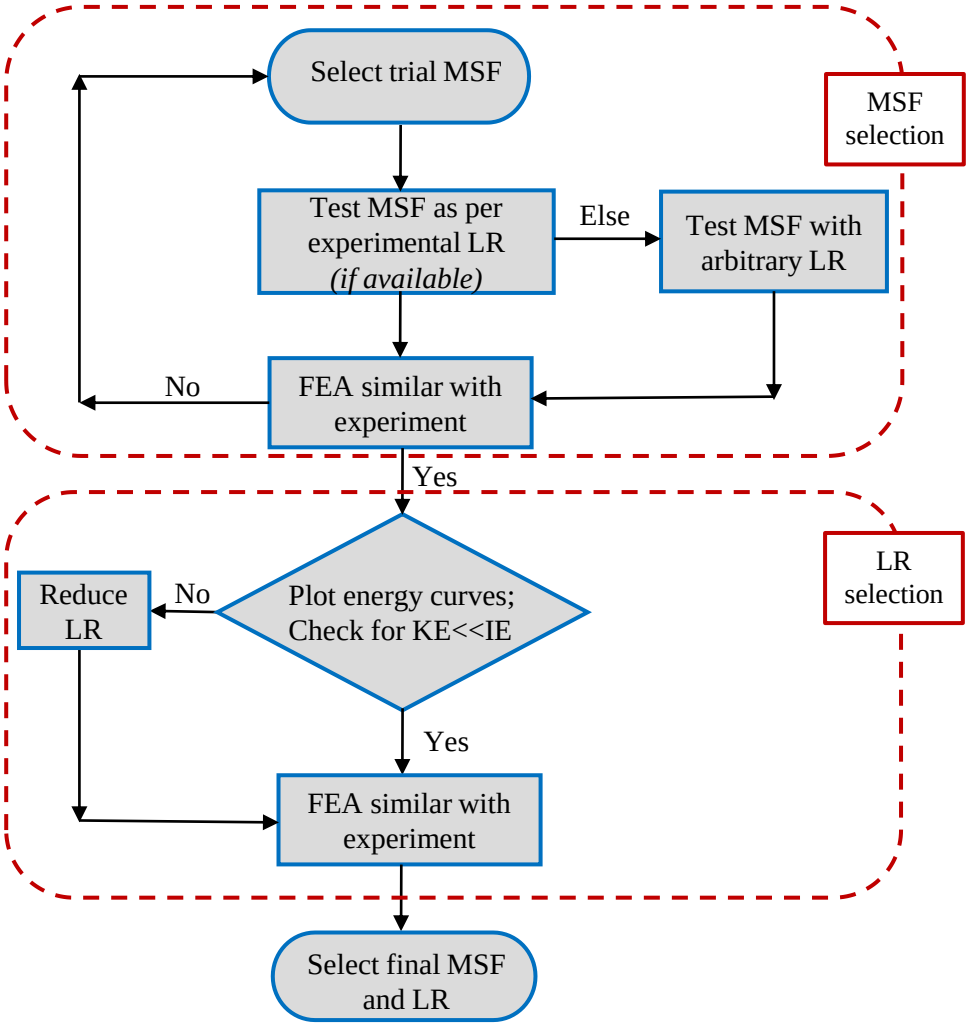

Fig. 30. Flow chart for determining MSF and LR.

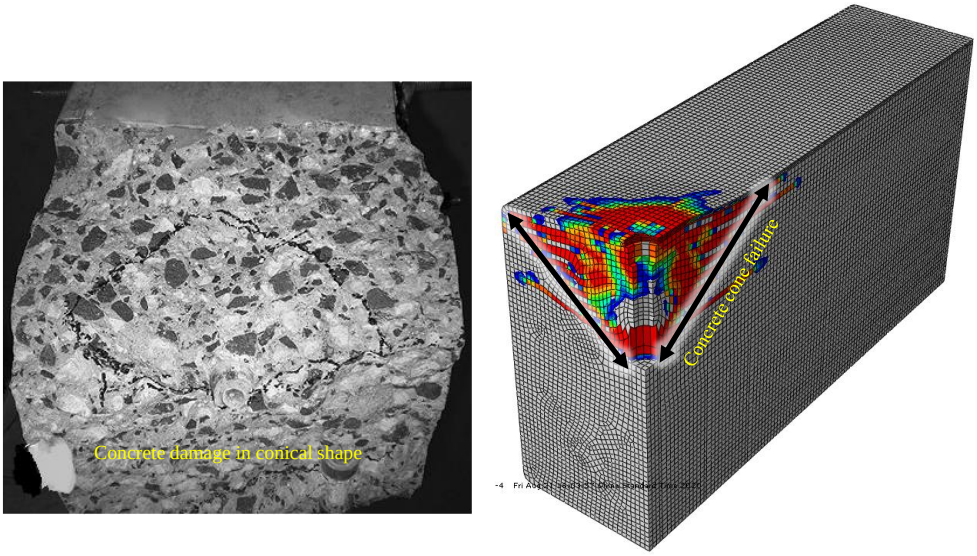

Fig. 31. Concrete cone developed in experiment vs FE quarter model for the specimen A-1M20-Mid [22] using HABB.

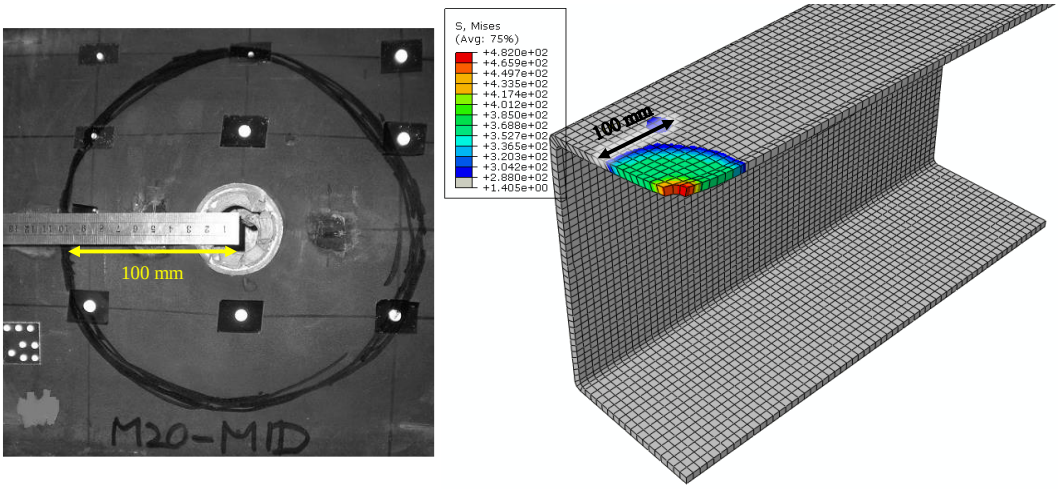

Fig. 32. Deformation of tube wall in experiment vs FE quarter model for the specimen A-1M20-Mid [22].

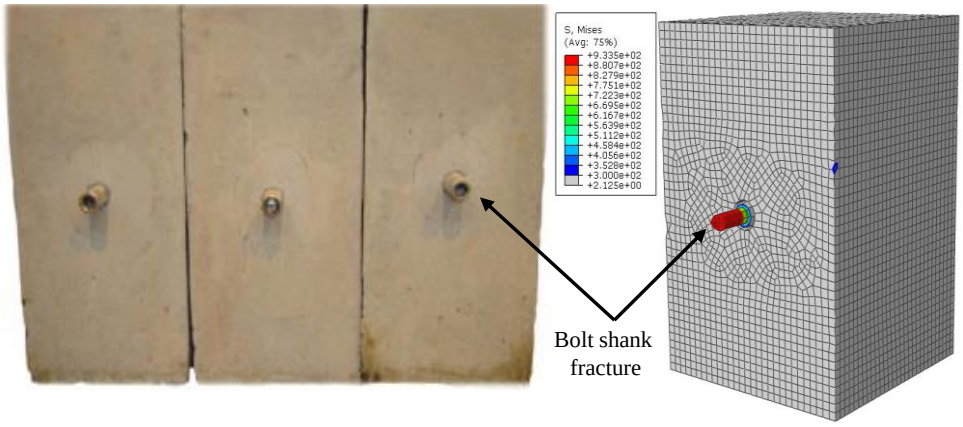

Fig. 33. Bolt fracture in experiment vs FE model for the specimen EHB16-150-8.8D-C40-1 [24].

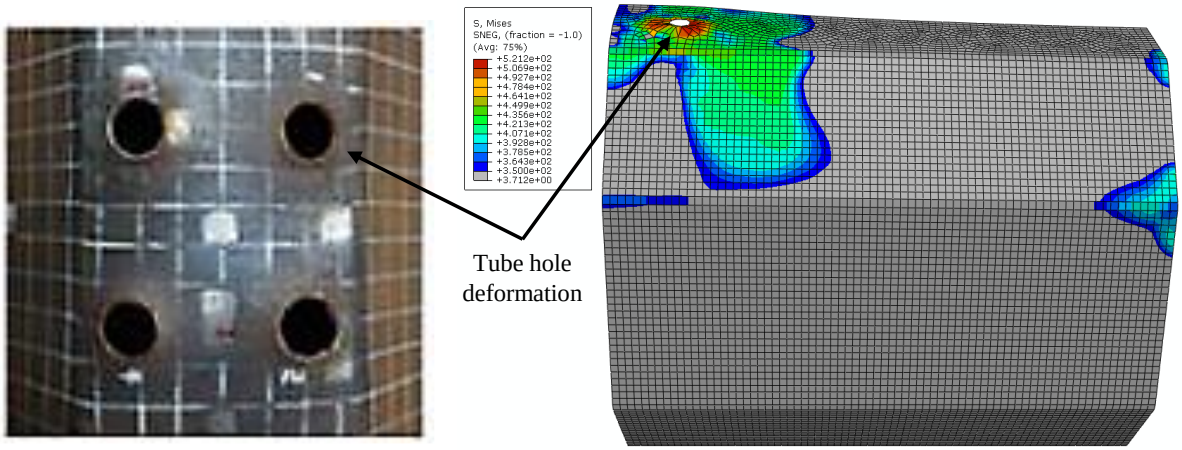

Fig. 34. Yielding of tube and bolt hole deformation in experiment vs FE quarter model for specimen Oct-W150-T4-S [30] using SCBB.

Table 1. Comparison of simulation time based on bolt mesh size.

Test model: EHB20-150-8.8F-C40-2 [24]			
Mesh size (mm)	5	7	8
No. of elements in bolt component	1962	1008	644
CPU time required (minutes)	63.35	22.56	15.75

Table 2. Comparison of fracture energy models.

Concrete strength (N/mm^2)		Fracture Energy, G_F (N/m)			
f_{ck}	f_{cm}	CEB-FIP Model Code (1993)	Trunk and Wittman (1998)	*fib* Bulletin 42 (2008)	CEB-FIP Model Code (2010)
50	58	88.99	168.39	156.10	151.61